VIBRATION INDUCED PERTURBATIONS

IN FLOW TROUGH CLOSED CONDUITS

A thesis Submitted
In partial Fulfillment of the Requirements
For The Degree
Of

Master of Technology

By

Kumaresh Bagchi
Y3101021

to the

Department of Aerospace Engineering
Indian Institute of Technology Kanpur
Kalyanpur, Kanpur

July, 2005

CERTIFICATE

It is certified that the work contained in the thesis entitled "**Vibration Induced Perturbations in Flow through Closed Conduits**", by **Kumaresh Bagchi**, has been carried out under my supervision and that this work has not been submitted elsewhere for a degree.

Dr. Abihijit Kushari
Assistant Professor
Department of Aerospace Engineering
Indian Institute of Technology Kanpur
Kalyanpur, Kanpur 208016

July 2005

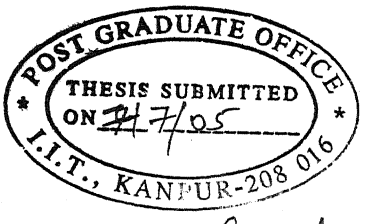

ABSTRACT

An effort has been directed towards exploring the dynamical property changes that affect a fluid flowing through a pipe when the pipe is under transverse vibration. Experiments have been carried out to observe the pressure changes taking place inside the fluid medium during oscillatory motion of the flow domain and then the data is analyzed using MATLAB. The pressure drop patterns are studied in detailed, in both time domain and frequency domain, as are the general behaviour of the mean pressure values at prescribed locations along the axial length of the pipe. Some effort has been made towards trying to characterize the mean pressure behaviour and its dependency on the characteristics of the oscillation of the pipe. The reflection of the fluid-structure interaction present has been spotted whenever observable. A simple Navier-Stokes solver also has been written to simulate, under restrictive boundary conditions, some features of a two-dimensional flow between two sinusoidally oscillating parallel plates of infinite expanse.

Dedicated to

My Parents and My Brother

&

ALLAH

ACKNOWLEDGEMENT

At this event of completion of my Master's Thesis, I experience feelings of achievement and some satisfaction. I wish to express my deep gratitude to all those who have helped me in all possible ways during my short tenure at IIT Kanpur.

I take this opportunity to sincerely thank my supervisor Dr. Kushari for his invaluable guidance, effective suggestions and constant encouragements. I am especially thankful to him for the patient ear that he lent me all through my work, and the valuable time of which there cannot be any count he wasted listening to the most mundane concerns of my wandering mind that was barely focused anytime. I am absolutely indebted for the endless hours of counseling that he would provide me almost as a friend and putting up with my unorganized way of working, if at all. I feel extremely privileged having met such gem of a person. My sincerest gratitude is reserved for him.

I must mention the most valuable role played by dear friend Sanjeev (Mr. Sanjeev Gupta), Mr. Rawat and his team, namely Kamlesh, Rajju, Sharad, Shyam and Premji in carrying out the experiments. I am very much thankful for the days and nights they have put up with me for the experiments to progress at the cost of their family lives. Also, my sincere appreciation goes towards Mr. Ravi and Mr. Avdesh Katiyar for the important parts they played to get the experiments up and running.

I am also thankful to my seniors Arnabda (Mr. Arnab Kr. De) and Subhankarda (Mr. Subhankar Sen) for the helping hands they extended whenever I needed them. My Thesis would not have been complete without their generous help.

I am also thankful to all the persons I have been associated with in here for making my stay here enjoyable. Meeting persons like Sanjoy Saha, Kanchan Dutta, Srinibas Karmakar, Md. Rabius Sunny, Amit Maji,(All of whom have been my batchmates here) Mr. Sishupal Singh, Mr. Sushil Tiwari have been absolutely memorable.

Finally, I would like to thank my parents and my brother for their blessings, constant encouragements and emotional support during all part of my Thesis preparation.

Contents

List of Figures

Figure No. and Name **Page No.**

INTRODUCTION

"*Vibration or agitation conditions imposed on supply system lines and associated components is probably the most ignored design consideration that could render as inadequate an otherwise good system.*

Due to the complex and important role played by the aircraft structures it is recommended that all rigid fuel supply lines vibratory responses be surveyed with the engine(s) in operation."

----The Experimental Aircraft Association

http://www.eaa.org/education/fuel/recommended_practices.html

The studies on fluid-structure interaction with emphasis on the structural effects of a piping system under vibration conveying fluid or such kind of problems involving structural aspects of a fluid carrying pipe line are aplenty. However, investigations focused on the effect of structural vibration on the fluid flowing inside that are reported are very limited in number. For that reason, literature available on the fluidic aspects of systems under vibration is limited.

The issue of effect of fluid when it is associated with moving boundaries was contemplated upon by Stokes in one of his celebrated paper in 1851, which has now come to be called "Stoke's Second Problem". Considering the case of fluid flowing over an infinite plate which is oscillating with a frequency ω such that at the wall, with the fluid I the far field at rest i.e. $u(\infty,t)=0$, $u(0,t)=U_0\cos\omega t$. The above is called the Stokes' second problem, after a celebrated paper by Stokes (1851). Assuming that $v=0, w=0$, the momentum equation becomes

$$\frac{\partial u}{\partial t}=-\frac{1}{\rho}+\nu\left(\frac{\partial^2 u}{\partial y^2}+\frac{\partial^2 u}{\partial z^2}\right)$$

Now, the pressure gradient can only be a function of time for this flow and hence can be absorbed into the velocity by a change of variables. Defining

$$u' = u + \int \frac{1}{\rho}\frac{dp}{dx}dt$$

Then

$$\frac{\partial u'}{\partial t} = \nu\left(\frac{\partial^2 u}{\partial y^2} + \frac{\partial^2 u}{\partial z^2}\right)$$

The above is the homogeneous heat conduction equation and a wealth of unsteady solutions is known. Now, the steadily oscillating solution to the above equation must be of the form $u(y,t) = f(y)e^{i\omega t}$, where $i = \sqrt{-1}$. Substituting that in the above equation we get the following ordinary differential equation

$$\frac{\partial^2 f}{\partial y^2} - \frac{i\omega}{\nu} f = 0$$

And the solution of which is of the form f=$\exp[-y\sqrt{\frac{i\omega}{\nu}}]$. u may be split into real and imaginary components. If the wall is oscillating, the final result is η

$$u_1 = U_0 \exp[-\eta]\cos(\omega t - \eta) \qquad \eta = y\sqrt{\frac{\omega}{2\nu}}$$

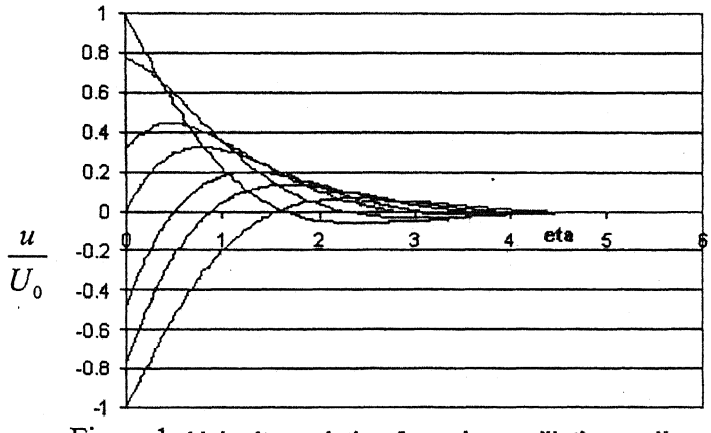

Figure1: **Velocity variation from the oscillating wall**

One very interesting phenomena can be observed here, that of u velocity changing signs to negatives at times, which indicates a flow reversal and hence possible formation of eddies if oscillation is affected onto two parallel plates in between whom there would be fluid present. That might result in severe pressure drops in pockets of

flow domain and that could cause problems in terms of, for example, an ensuing two phase flow through fuel supply line of an aircraft engine.

The waves created in the fluid by the moving wall lag behind in phase and damp out as y increases. The thickness δ of oscillating layer can again be defined where $\frac{u}{U_0}$=0.01, that is where $e^{-\eta}$=0.01 or η=4.6.

Solving for y, $\delta = 6.5\sqrt{\frac{\nu}{\omega}}$.

Again we have the characteristic laminar flow dependence upon $\sqrt{\nu}$. For air at 20^0 C with a plate frequency of 1 Hz ($\omega = 2\pi$ rad/s), we compute $\delta \approx 1$cm. The wall shear stress at the oscillating wall is given by

$$\tau_w = \mu(\frac{du}{dy})_w = U_0\sqrt{\rho\omega\mu}\sin(\omega t - \frac{\pi}{4})$$

And thus the maximum shear lags the maximum velocity by 135^0.

Now, the following dependence of the velocity pattern can be noticed when the fluid concerned is changed from water to air. The following plots were generated between two plates oscillating simultaneously together and the distance between them being 10 mm. The most notable property change that will be affected from changing to air from water is the effect of lower viscosity and thus the velocity perturbations damp out at much farther distances from the wall.

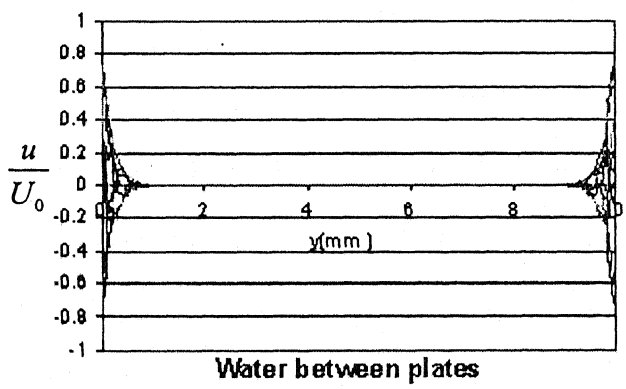

Water between plates

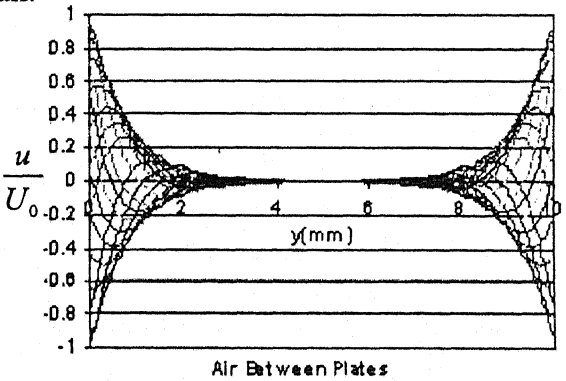

Air Between Plates

Now let us consider the effect of frequency of oscillation of the plates when air is the fluid medium between the two. Air is considered for the plots because the effects of oscillations are more pronounced in case of air.

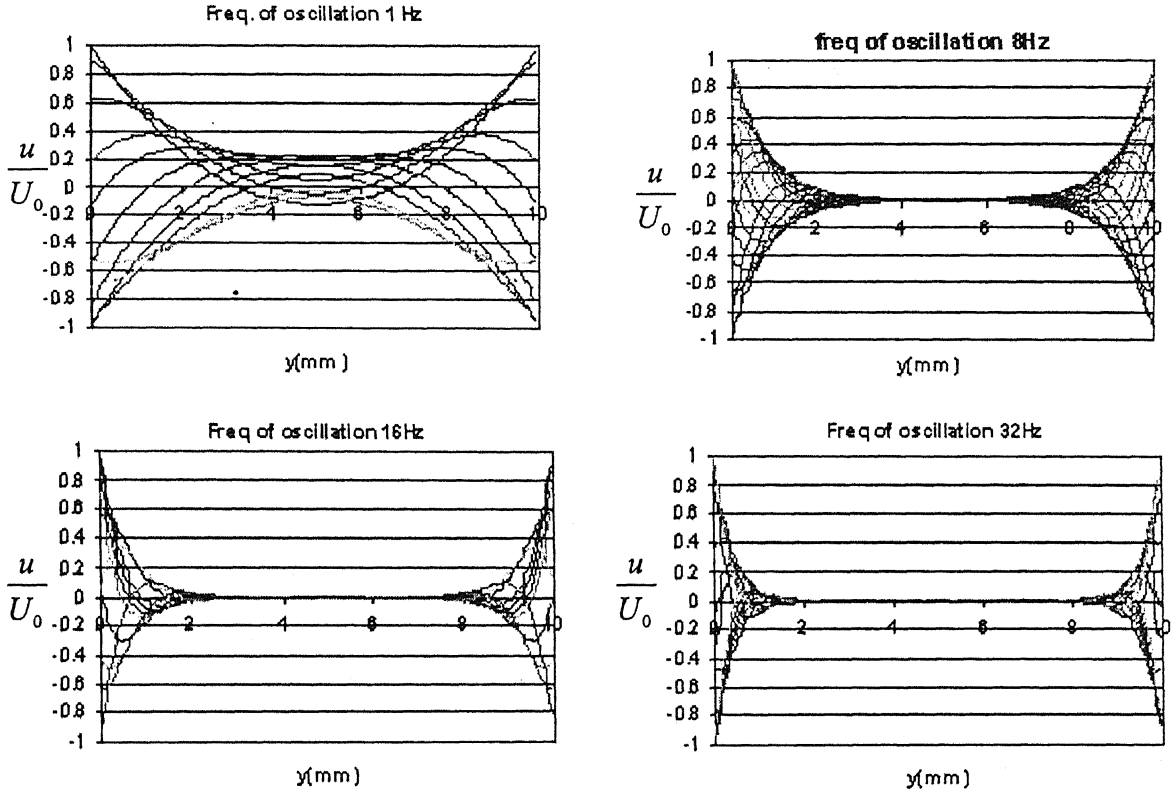

Figure2: Effect of frequency of oscillation on u velocity

The effect of oscillation frequency of the plates on the fluid in between them is very apparent. As frequency of oscillation goes up, the perturbations in the u velocity goes down and limits itself in regions more and more close to the plates. In essence, the higher oscillation frequency has a damping effect on the perturbation produced in the fluid. As will be pointed out later, the same effect has been seen while carrying the experimentations as well as in the computational results. This phenomenon can perhaps be explained on the lines that as oscillation frequency of the neighboring wall goes up, the fluid particle has less time to "absorb" the effect of the momentum being transmitted to it and transmit to other neighboring fluid particles farther from the wall and then again adjusting to the lack of momentum available due

to the evacuating effect that would be there as the wall moves away. So, the perturbations don't get enough time to settle down and their net effect goes down as oscillation frequency goes up.

J. C. Mishra et al [1] have solved the incompressible Navier Stokes equation in two dimensions in the vorticity-streamfunction formulation for the unsteady flow of an incompressible viscous fluid in the entrance region of a parallel-sided channel whose walls pulsate in a prescribed manner. The problem is different from the present case in the sense that the walls move symmetrically about the central axis. They have shown that for large values of frequency of pulsation f_0 of the channel walls oscillating sinusoidally with time, back flow occurs near the channel walls at a certain location far downstream from the entrance section at a certain instant of time. It is also found that at a subsequent time there is flow reversal at the same location across the entire cross-section of the channel. However, they have shown that for sufficiently small values of f_0, such back flow does not occur.

Tienfuan Kehr et al [2] have numerically simulated a fluid-structure interaction problem with significant focus on the effect of fluid of a moving structural boundary as in a cross-connection control valve. Modeling the governing equations for both solid and the fluid and the solid using consistent penalty function finite element method with Newmark approach for laminar flow situations. They have shown that the movement of the structural components, which were treated as moving boundaries in computation, has a large bearing on the fluid medium.

D Mateescu and D. A. Venditti [3] developed techniques for effectively simulating flows with moving/oscillating boundaries using time dependent co-ordinate transformation and usage of artificial compressibility thereby solving the moving boundary problem in a static domain. They have validated the efficacy of the code by comparing with experimental results for the flow over a backward facing step with an oscillating wall immediately following the step. They have extended the application of the formulation (Mateescu et al. [4]) to the simulation of laminar three-dimensional flows between annular passages with the outer cylinder oscillating and the inner cylinder remaining fixed in cylindrical coordinate systems. The inner cylinder geometry was taken both as uniform and with a backward facing step. In the fixed computational grid obtained by the coordinate transformation, their method is based on a three-time-level implicit scheme for the time-accurate integration of the Navier-Stokes equations, and uses a pseudo-time integration with artificial compressibility based on an implicit Euler scheme to advance the solution to a new real-time level. It uses a finite-difference spatial discretization based on a stretched staggered grid, as well as a factored ADI scheme to reduce the problem to computationally efficient solutions of scalar tridiagonal systems of equations. They have compared the results with previous results with smaller amplitudes of oscillation of the outer cylinder as well as with experimental cases. They have not done any formulation for a turbulent flow situation though. They found that the nonlinear unsteady fluid forces calculated with this method depend on both the displacement and the velocity of the oscillating structural boundary, in agreement with physical reality, but in contrast with the linear ones obtained by mean-position analyses based on the small amplitude assumption, which are only velocity-dependent.

Abdelkader Frendi [5] has numerically investigated the effect of structural oscillation on fluid dynamics using a fully coupled model that solves the unsteady flow equations as well as the dynamic equations of the structure. In all the flow regimes studied, laminar, transitional and turbulent, he has reported that the structural vibration introduces significant changes in the flow field. While investigating the flow geometry of a backward facing step with an immediately following oscillating bottom wall, the size and shape of the various recirculation bubbles is found to be strongly affected and oscillate at the same frequency as that of the structure. In addition, the reattachment point oscillates at the same frequency as that of the structural vibrations.

B. Benhamou et al. [6] have carried out experimentations to visualize the developing flow (transition to turbulence mainly) in a pipe forced to oscillate in a horizontal plane. The visualization results show that pipe oscillations induce a secondary transversal flow as indicated by the helicoidal form of the streak lines. At relatively high oscillation frequencies, the intensity of this transversal flow increases and may destabilize the flow structure. In fact, large mixing is induced in the flow and leads to the development of turbulent vortices even when the flow Reynolds number is lower than its critical transition value for a stationary pipe ($Re < 2000$). This earlier transition to turbulence, attributed to the Coriolis force, occurs at lower values of Re as the oscillation Reynolds number, indicated as $Re\omega$, increases. The flow structure can become fully turbulent if $Re\omega$ is further increased. They have developed a chart indicating the limits of the transition and full turbulent flow structures.

Significant amount of work has been carried out on pulsatile pipe flow in which the axial velocity component has an unsteady, often periodic component

imposed on it. A good reference on the state of the art was found on the review paper by Melda Ozdinc et al. [7].

Some comprehensive list of articles on general fluid structure interaction phenomena can be obtained in the review paper by A. S. Tjjeseling [8]. In there, a review of literature on transient phenomena in liquid-filled pipe systems is presented. Waterhammer, cavitation, structural dynamics and fluid-structure interaction (FSI) are the subjects dealt with. The emphasis is on the history of FSI research in the time-domain. Some surveys of mathematical models and experimental results have been provided there.

Numerical formulation:

In order to see what happens to a fluid when the wall near it is having oscillations, the two-dimensional Navier-Stokes equations in the conservative form are solved numerically for the flow between two infinite parallel plates. For doing so, the well known semi explicit scheme SMAC (Simplified Marker and Cell) is used. Given below is a description of how the solver was constructed.

Governing Equations:

In Cartesian Coordinates, the governing equations for incompressible two-dimensional laminar flow are

Continuity Equation:

$$\frac{\partial u^*}{\partial x^*}+\frac{\partial v^*}{\partial y^*}=0$$

x-momentum equation:

$$\frac{\partial u^*}{\partial t^*}+\frac{\partial (u^{*2})}{\partial x^*}+\frac{\partial (v^*u^*)}{\partial y^*}=-\frac{1}{\rho}\frac{\partial (p^*)}{\partial y^*}+\nu(\frac{\partial^2 u^*}{\partial x^{*2}}+\frac{\partial^2 u^*}{\partial y^{*2}})$$

y-momentum equation:

$$\frac{\partial v^*}{\partial t^*}+\frac{\partial (u^*v^*)}{\partial x^*}+\frac{\partial (v^{*2})}{\partial y^*}=-\frac{1}{\rho}\frac{\partial (p^*)}{\partial y^*}+\nu(\frac{\partial^2 \upsilon^*}{\partial x^{*2}}+\frac{\partial^2 \upsilon^*}{\partial y^{*2}})$$

The above equations are normalized by the following substitutions:

$$x=\frac{x^*}{D}\quad y=\frac{y^*}{D}\quad u=\frac{u^*}{U}\quad v=\frac{v^*}{U}\quad p=\frac{p^*}{\rho U^2}\quad t=\frac{t^*}{D/U}$$

Then, Continuity Equation:

$$\frac{\partial u}{\partial x}+\frac{\partial v}{\partial y}=0$$

x-momentum equation:

$$\frac{\partial u}{\partial t}+\frac{\partial (u^2)}{\partial x}+\frac{\partial (vu)}{\partial y}=-\frac{\partial p}{\partial y}+\frac{1}{\mathrm{Re}}(\frac{\partial^2 u}{\partial x^2}+\frac{\partial^2 u}{\partial y^2})$$

y-momentum equation:

$$\frac{\partial v}{\partial t}+\frac{\partial(uv)}{\partial x}+\frac{\partial(v^2)}{\partial y}=-\frac{\partial(p)}{\partial y}+\frac{1}{\mathrm{Re}}(\frac{\partial^2 \upsilon}{\partial x^2}+\frac{\partial^2 \upsilon}{\partial y^2})$$

The Staggered Grid

As it has been seen, the major difficulty encountered in the solution of the incompressible flow is the non-availability of any obvious equation for pressure.A staggered grid is often used with pressure correction schemes. The idea is to define a different grid for each velocity component. The main advantage of this method is its capacity to perform corrections for both velocity and pressure factors at once. The mass flow can be calculated without any interpolation for the relevant velocity component. In the staggered grid, the velocity components are calculated for the points that lie on the faces of the cells. A two dimensional grid pattern is shown below

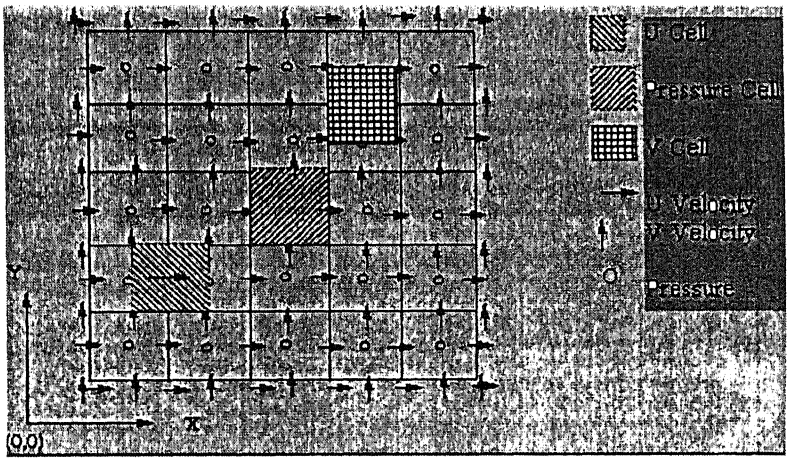

Figure3: Arrangement of velocity and pressure nodes in a two-dimensional mesh

The u and v velocities are normal to the faces on which they are defined. If uniform grids are used, the locations are exactly midway between two adjacent grid points. In such arrangements, the pressure difference between two adjacent cells is the driving force for the velocity component located between the interfaces of these cells.

Solution Procedure:

Now, expressing the momentum and continuity equations at the indicative time levels (indicated by the superscripts n and n+1):

x-momentum equation:

$$\frac{u^{n+1}-u^n}{\Delta t}+\left[\frac{\partial(u^2)}{\partial x}+\frac{\partial(vu)}{\partial y}\right]^n=-\left(\frac{\partial p}{\partial y}\right)^{n+1}+\frac{1}{\mathrm{Re}}\left(\frac{\partial^2 u}{\partial x^2}+\frac{\partial^2 u}{\partial y^2}\right)^n \quad \text{.....(a)}$$

y-momentum equation:

$$\frac{v^{n+1}-v^n}{\Delta t}+\left[\frac{\partial(uv)}{\partial x}+\frac{\partial(v^2)}{\partial y}\right]^n=-\left(\frac{\partial p}{\partial y}\right)^{n+1}+\frac{1}{\mathrm{Re}}\left(\frac{\partial^2 \upsilon}{\partial x^2}+\frac{\partial^2 \upsilon}{\partial y^2}\right)^n \quad \text{.....(b)}$$

Continuity Equation:

$$\left[\frac{\partial u}{\partial x}+\frac{\partial v}{\partial y}\right]^{n+1}=0$$

The continuity equations are satisfied at the $(n+1)^{th}$ time level because the continuity should act as the constraint for the new solutions obtained from the momentum equations (it is meaningless to apply it at the already known nth time level). Since the three equations are to be solved simultaneously, the velocity field cannot be solved in a fully explicit way.

The solution procedure follows the well known two step "predictor-corrector" process.

"Predictor Step"

Indicating the predicted properties with * as superscript from here onwards,

$$\frac{u^{n+1}-u^*}{\Delta t}+\left[\frac{\partial(u^2)}{\partial x}+\frac{\partial(vu)}{\partial y}\right]^n=-\left(\frac{\partial p}{\partial x}\right)^n+\frac{1}{\mathrm{Re}}\left(\frac{\partial^2 u}{\partial x^2}+\frac{\partial^2 u}{\partial y^2}\right)^n \quad \text{..... (a')}$$

$$\frac{v^{n+1}-v^*}{\Delta t}+\left[\frac{\partial(uv)}{\partial x}+\frac{\partial(v^2)}{\partial y}\right]^n=-\left(\frac{\partial p}{\partial y}\right)^n+\frac{1}{\mathrm{Re}}\left(\frac{\partial^2 \upsilon}{\partial x^2}+\frac{\partial^2 \upsilon}{\partial y^2}\right)^n \quad \text{..... (b')}$$

Subtracting (a') from (a)

$$\frac{u^{n+1}-u^*}{\Delta t}=\frac{\partial\left(p^{n+1}-p^n\right)}{\partial x}$$

Subtracting (b') from (b)

$$\frac{v^{n+1}-v^*}{\Delta t}=\frac{\partial\left(p^{n+1}-p^n\right)}{\partial y}$$

Defining

$$u'=u^{n+1}-u^*$$

$$v'=v^{n+1}-v^*$$

$$p'=p^{n+1}-p^*$$

we have $u'=-\Delta t\frac{\partial p'}{\partial x}$ and $v'=-\Delta t\frac{\partial p'}{\partial y}$ so that

$$u^{n+1}=u^*-\Delta t\frac{\partial p'}{\partial x} \quad \text{and} \quad v^{n+1}=v^*-\Delta t\frac{\partial p'}{\partial y} \qquad \text{.....(c)}$$

Putting the above in the continuity equation, we get

$$\left(\frac{\partial u}{\partial x}\right)^{n+1}+\left(\frac{\partial v}{\partial y}\right)^{n+1}=0$$

$$\Rightarrow \frac{\partial^2 p'}{\partial x^2}+\frac{\partial^2 p'}{\partial y^2}=\frac{1}{\Delta t}\left(\frac{\partial u^*}{\partial x}+\frac{\partial v^*}{\partial y}\right) \qquad \text{.....(c)}$$

The above is a Poisson's Equation whose right hand side is known as u^* is known in the predictor step.

"Corrector Step"

In this step the followings were done:

1. Solution of the Poisson Equation for pressure (c) using GS-SOR (Gauss-Siedel Successive Over Relaxation) scheme as this is one of the most computationally efficient method of solving the Poisson's equation in CFD. The convergence

criteria for the magnitude of residue was set at 1e-6 and the over relaxation factor was set at 1.3 after numerical experimentation.

2. Using the pressure correction obtained in the last step, u^{n+1} and v^{n+1} was computed. But since it is not known if the obtained velocity values would satisfy the continuity equations, they were still treated as "better guesses" u^* and v^* such that $u^* = u^* - \Delta t \frac{\partial p'}{\partial x}$ and $v^* = v^* - \Delta t \frac{\partial p'}{\partial y}$

3. Now the divergence of the velocity field (continuity equation) is calculated with the just obtained newer guesses.

4. If $\|\text{Divergence(Velocity field)}\| < \varepsilon$ then $u^{n+1} = u^*$ and $v^{n+1} = v^*$. Else we go back again to step 1 of corrector step. The value of ε was chosen as 1e-5 in the present work.

Treatment of Boundary Condition

At the predictor step, u^* and v^* should satisfy the boundary condition for u^{n+1} and v^{n+1} respectively and at the corrector step, both pressure and velocity boundary conditions are implemented. While applying the pressure boundary conditions, instead of the true pressure boundary condition, the boundary condition is applied on the pressure correction.

For the implementation of the boundary conditions, the standard approach of a layer of fictitious cells of unit cell thickness all around the main computational domain was assumed. The boundary conditions were imposed at the fictitious cells and the main computations were carried out on the physical computational domain.

The following boundary conditions were imposed:

1. At the solid walls:

"No-slip" boundary condition for the velocities was imposed. That was achieved in the following way. In the bottom or top walls, where u velocities were parallel to the wall, average of the u velocities immediately adjacent to the wall were averaged to zero or wall velocity in case of wall moving in the x direction. Taking (0,0) point to be located at the bottom left corner of the mesh, $\frac{u(i,1)+u(i,2)}{2}=u_{wall}$ or $u(i,1)=2*u_{wall}-u(i,2)$ for the bottom wall(u_{wall}=0.0 for static walls) and likewise for the other wall. Velocity components perpendicular to the wall were also made zero. For example, on the bottom wall, v velocity being perpendicular to the bottom wall, $v(i,1)=0.0$, and so on.

2. Pressure correction boundary condition:

Neumann boundary condition of $\frac{\partial p'}{\partial \eta}=0$ where η represents normal direction to any solid wall and any velocity specified boundary was implemented at the solid walls.

Dirichlet boundary condition of $p'=0$ was adopted where pressure value could be known, e.g. the inlet and outlet boundary conditions for flow through a pipe or flow over a backward facing step.

3. The outlet boundary condition for convected parameters:

So that the quantities may retain their properties while going convected out of the computational domain and not vice-versa, Orlanski outflow condition in the x-direction is imposed as follows.

$$\frac{\partial \phi}{\partial t}+U\frac{\partial \phi}{\partial x}=0$$

where ϕ is the convected scalar like u or v velocity, and U is the average stream velocity. In the present case, the implicit implementation/discretization of the above was done as follows:

$$\frac{u^{n+1}_{fictitious} - u^{n}_{fictitious}}{\Delta t} + U\frac{\left(u^{n+1}_{fictitious} - u^{n+1}_{real}\right)}{\Delta x} = 0$$

or,
$$u^{n+1}_{fictitious} = \frac{\left(u^{n}_{fictitious} + \frac{U\Delta t}{\Delta x}u^{n+1}_{real}\right)}{\left(1 + \frac{U\Delta t}{\Delta x}\right)}$$

Discretization

Considering one convective term in the NS equation: $\frac{d(u\phi)}{\partial x}$

Here u is the convecting vector and ϕ is the convected scalar (u in the x-momentum and v in the y momentum equation respectively)

Considering grid locations,

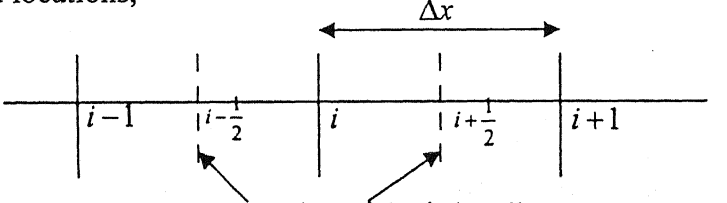

Virtual boundaries of the i-th cell

$$\frac{d(u\phi)}{\partial x} = \frac{(u\phi)_{i+\frac{1}{2}} - (u\phi)_{i-\frac{1}{2}}}{\Delta x}$$

$$= \frac{(u)_{i+\frac{1}{2}}(\phi)_{i+\frac{1}{2}} - (u)_{i-\frac{1}{2}}(\phi)_{i-\frac{1}{2}}}{\Delta x}$$

First Order Upwind Scheme:

$$\text{If } u_{i+\frac{1}{2}} > 0, \quad \phi_{i+\frac{1}{2}} = \phi_i$$

$$\text{If } u_{i+\frac{1}{2}} < 0, \quad \phi_{i+\frac{1}{2}} = \phi_{i+1}$$

$$\text{If } u_{i-\frac{1}{2}} > 0, \quad \phi_{i-\frac{1}{2}} = \phi_{i-1}$$

$$\text{If } u_{i-\frac{1}{2}} < 0, \quad \phi_{i-\frac{1}{2}} = \phi_i$$

The above scheme is a first order accurate scheme but is very stable.

Central Differencing:

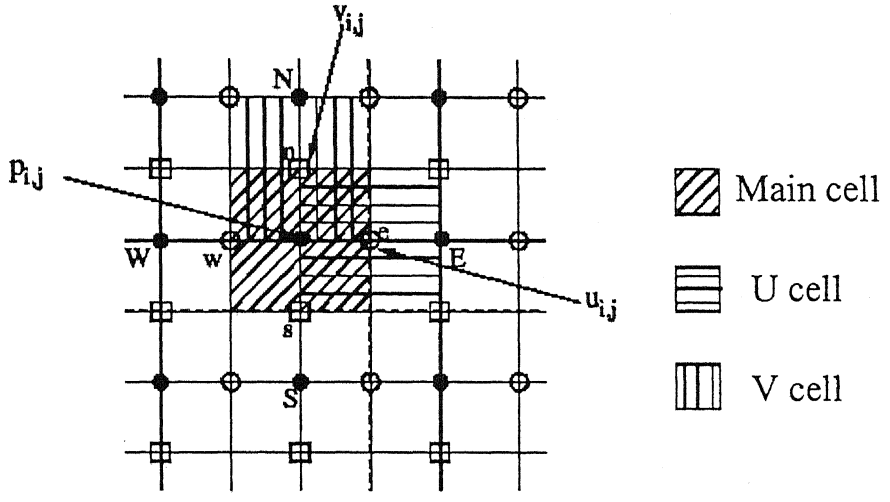

Figure4: The mesh arrangement and cell positions in central differencing

In central differencing we adopt the following form of discretization:

$$(u\phi)_{i+\frac{1}{2}} - (u\phi)_{i-\frac{1}{2}} = (u)_{i+\frac{1}{2}}(\phi)_{i+\frac{1}{2}} - (u)_{i-\frac{1}{2}}(\phi)_{i-\frac{1}{2}}$$

Depending on the momentum equation involved, the ϕ term is calculated on the faces of the u cell and v cell. For example, the discretized convective terms in x-momentum equation looks like the following (convective terms taken to the right):

```
-( ( 0.5*( u[i+1][j] + u[i][j] ) * 0.5 * ( u[i+1][j] + u[i][j] )
- 0.5 * ( u[i][j] + u[i-1][j] ) * 0.5 * ( u[i][j] + u[i-1][j] ) ) / dx )
```

```
-( 0.5 * ( u[i][j+1] + u[i][j] ) * 0.5 * ( v[i+1][j] + v[i][j] )
- 0.5 * ( u[i][j] + u[i][j-1] ) * 0.5 * ( v[i+1][j-1] + v[i][j-1] ) ) / dy      and so on.
```

The above scheme is second order accurate and due to better results obtained using this scheme on benchmark problems, the above scheme is used in solving the real flow situation under consideration.

Coordinates in rectilinear acceleration: Extended Galilean invariance

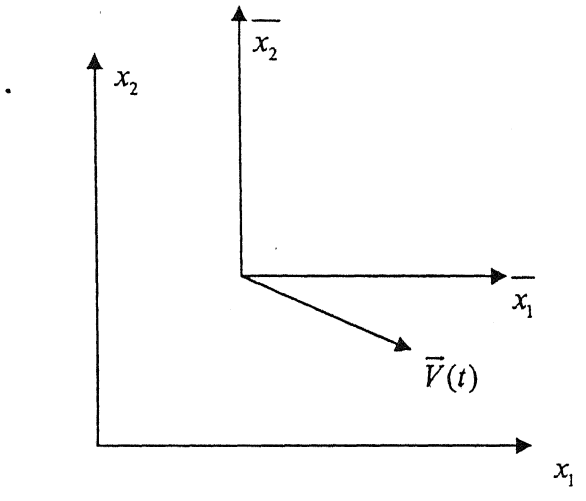

Figure 5: Inertial and non-inertial rectangular coordinate systems

Considering an inertial coordinate system x_1x_2 and a non-inertial system $\overline{x_1x_2}$ which is moving with a time dependent velocity $\vec{V}(t)$. The Navier-Stokes equation takes the following form in the non-inertial system:

$$\frac{\partial \overline{u_j}}{\partial t} + u_i \frac{\partial \overline{u_j}}{\partial \overline{x_i}} = \nu \frac{\partial^2 \overline{u_j}}{\partial \overline{x_i} \partial \overline{x_i}} - \frac{1}{\rho} \frac{\partial p}{\partial \overline{x_j}} - \overline{A_j} \quad \text{.....(d)}$$

where the additional term on the right hand side is the acceleration of the frame,

$$\overline{A_j} = \frac{d\vec{V}}{dt}$$

The last two terms can be written as

$$\frac{1}{\rho}\frac{\partial p}{\partial x_j} + \overrightarrow{A_j} = \frac{1}{\rho}\frac{\partial}{\partial x_j}(p + \rho \overrightarrow{x_i}\,\overrightarrow{A_i})$$

showing that frame acceleration can be absorbed in a modified pressure. Consequently, the Navier-Stokes equation when written in the transformed variables like scaled velocity

$\hat{u} = \frac{\vec{u}}{U}$ and modified pressure field $\hat{p} = \frac{(p + \rho \vec{x}.\vec{A})}{\rho U^2}$ etc will have a form identical to equation (d) even for the coordinate frame with arbitrary rectilinear acceleration. This is called extended Galilean Invariance.

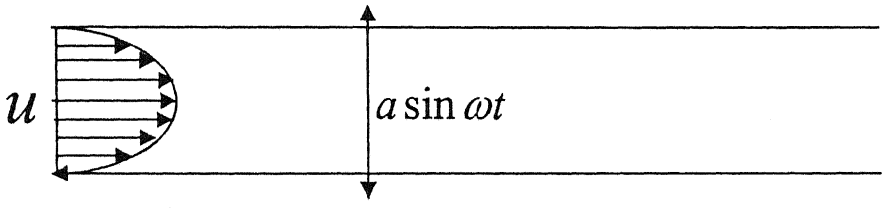

Figure6: 2-D incompressible flow between two parallel oscillating plates

In the present problem, we have 2-d flow between parallel plates, to model which we add $\frac{d^2(a\sin\omega t)}{dt^2}$ to the v-momentum equation after being nondimensionalized by dividing with ($U * n$).

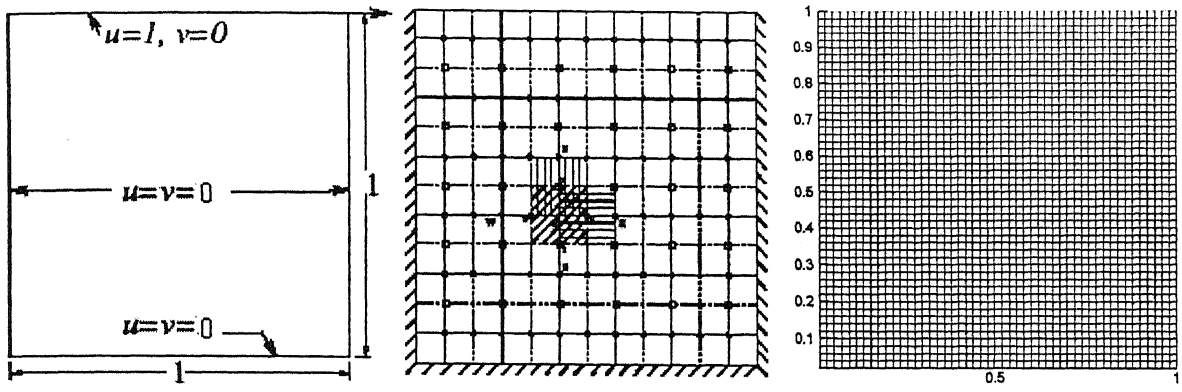

Figure7: (a) Geometry and boundary conditions of the cavity (b) Computational Cells (c) Computational Mesh

A lid driven cavity flow is the most commonly used computational experiment to demonstrate the performance of an incompressible Navier-Stokes solver. A comprehensive collection of results for different Reynolds number have been presented by Ghia et al [9]. Computation for the problem at hand has been performed with a 50X10 grid, so the benchmark problem also has been presented with a modest 50X50 grid but the results were compared with 129X129 grid.

The top wall of the cavity moves with a uniform velocity U causing a flow field affected by the viscous effect at the fluid-solid interface. The big vortex is called the primary vortex and the smaller vortices are called secondary vortices as shown in the following figures. The existence and size of the secondary vortices depend on the Reynolds number defined as

$$Re=\frac{UL}{\nu}$$

Results are plotted for Re=100, 400, 1000. For all calculations for the present solution, the timestep Δt is chosen as 10% of the value given by the minimum of that given by CFL (Courant- Fredrichs-Lewy) and GFN (Grid Fourier Number) criteria. The over-relaxation parameter in the Gauss-Siedel iterations for the pressure

correction was taken as 1.3 after experimentation. All computations are done on a 50X50 grid using SMAC scheme.

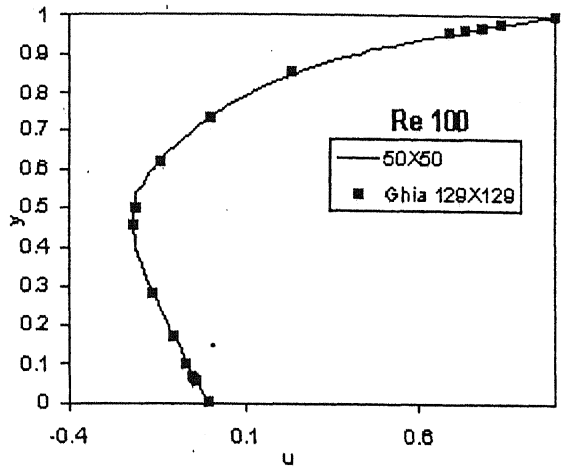

u-velocity along vertical centerline

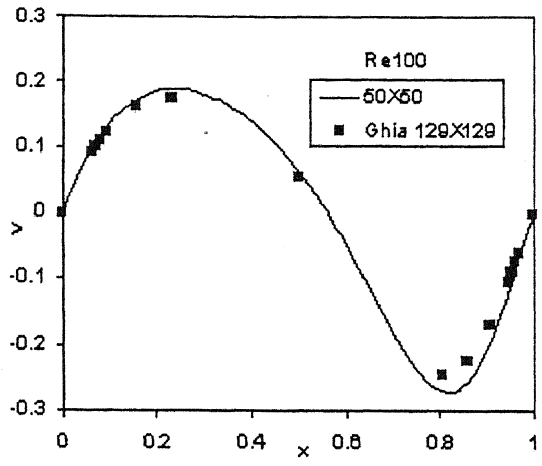

v-velocity along horizontal centerline

Figure8: Comparison of u and v velocity with Ghia er al [9].

The u velocity profile along the vertical centerline of cavity and u velocity profile along the horizontal centerline are shown in the figure above with the benchmark solution of Ghia et al[9] being included for comparison for different Reynolds numbers. The results are fairly in agreement with the benchmark solution, keeping in mind the number of grid points used (2500) is much less compared to the 16641 points which the benchmark calculation is arrived with. But the trends are very clearly visible. Two small counter rotating vortices (secondary vortices) are located in the lower corners and the right corner vortex is bigger than the right as shown in the streamline plots that follow.

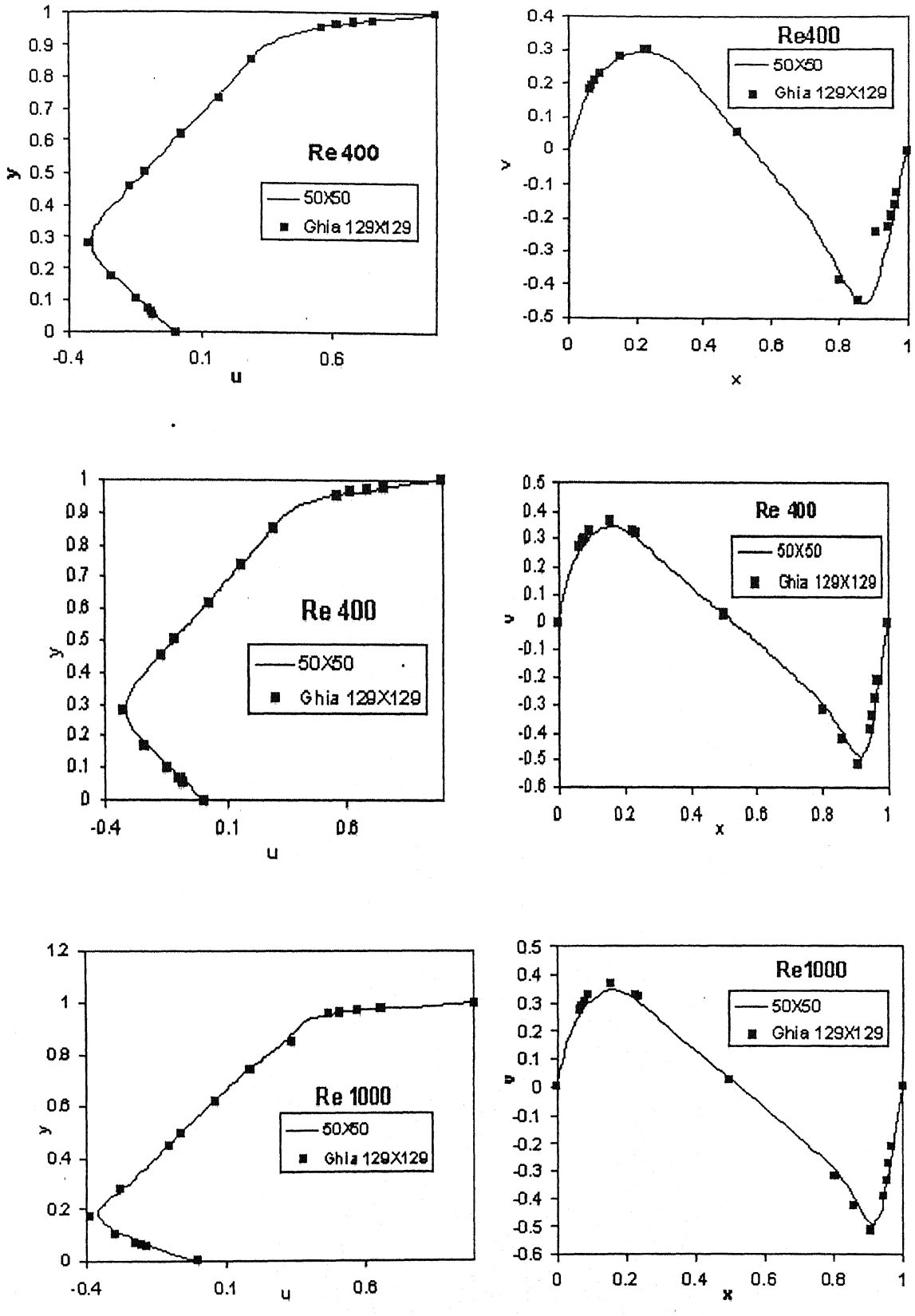

Figure9: Comparison of u and v velocity with Ghia et al[9].

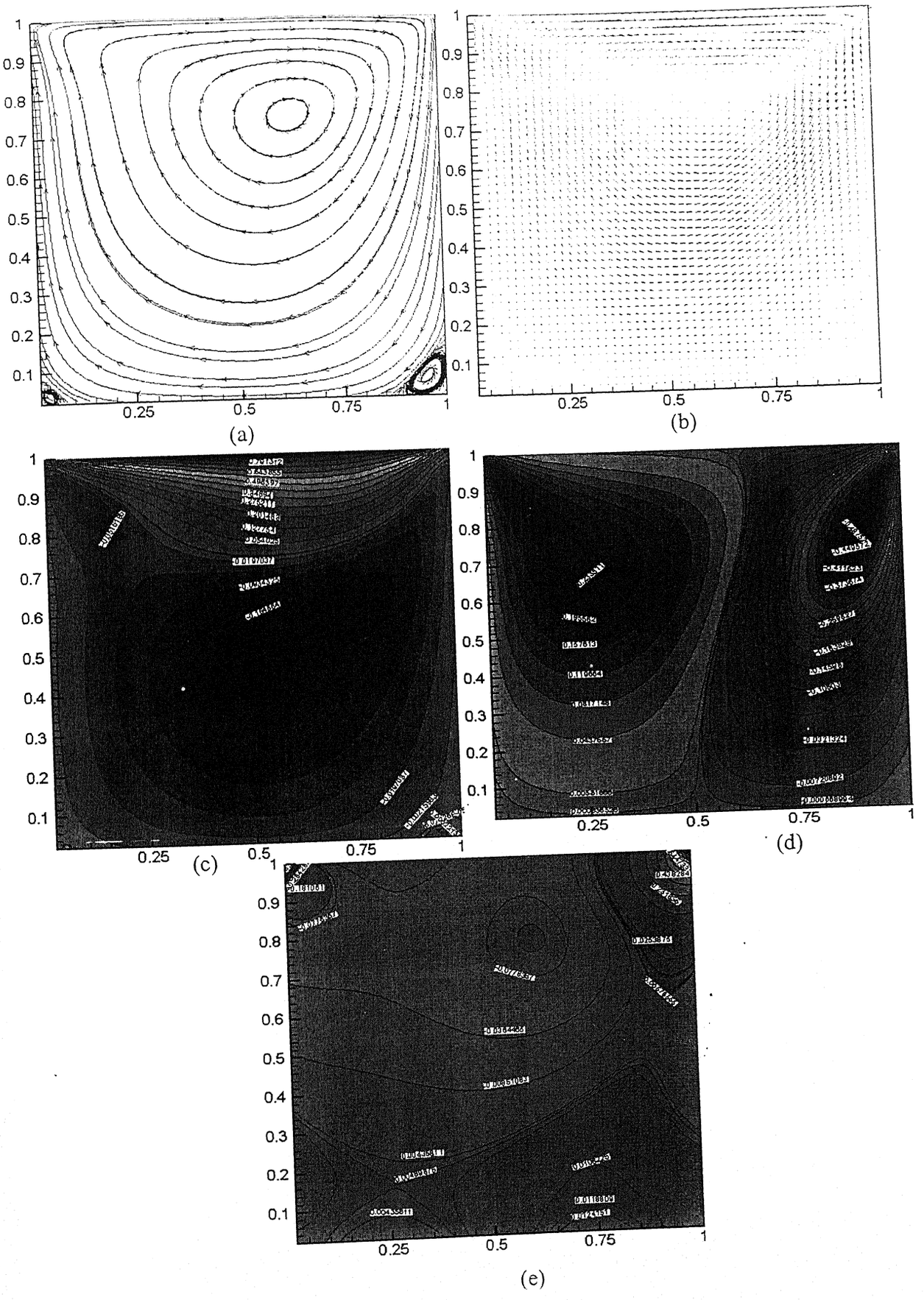

Figure10: *Re*=100 (a) streamlines (b) vectors (c) u-contour(d)v-contour (e) p-contour

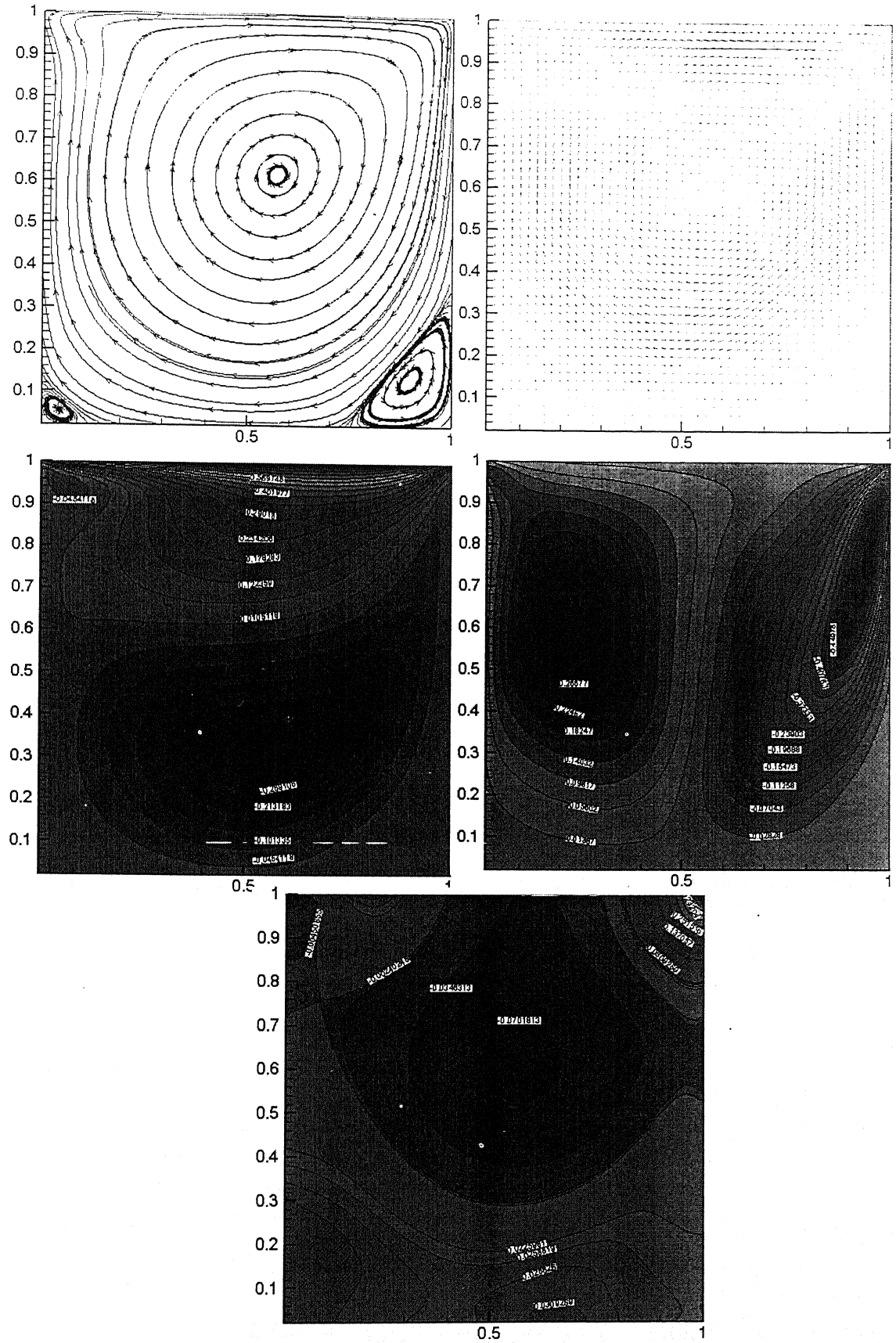

Figure11: (Left to right) *Re*=400 streamlines, vectors, u-contour, v-contour, p-contour

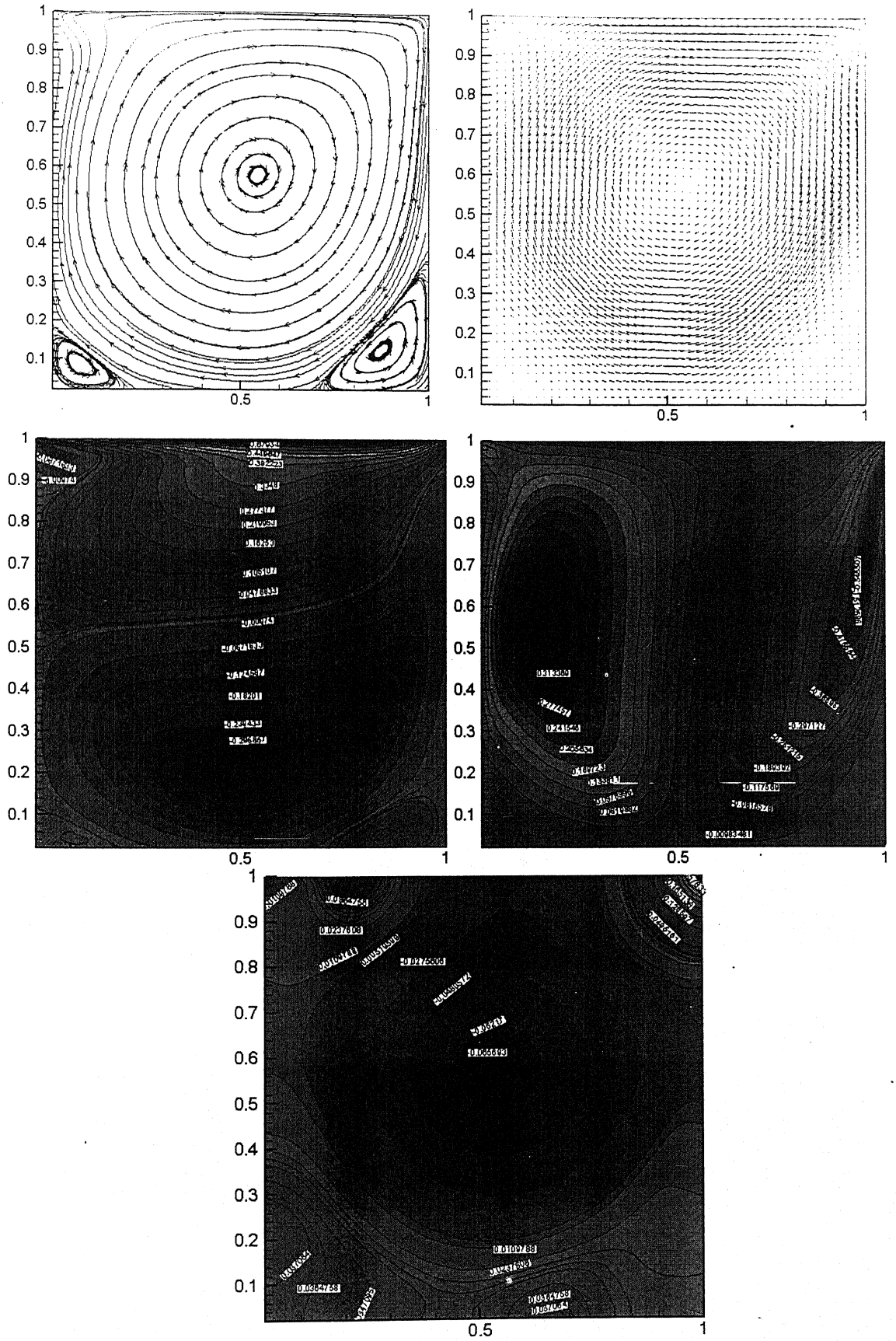

Figure12: (Left to right) *Re*=1000 streamlines, vectors, u-contour, v-contour, p-contour

Flow over a Backward Facing step:

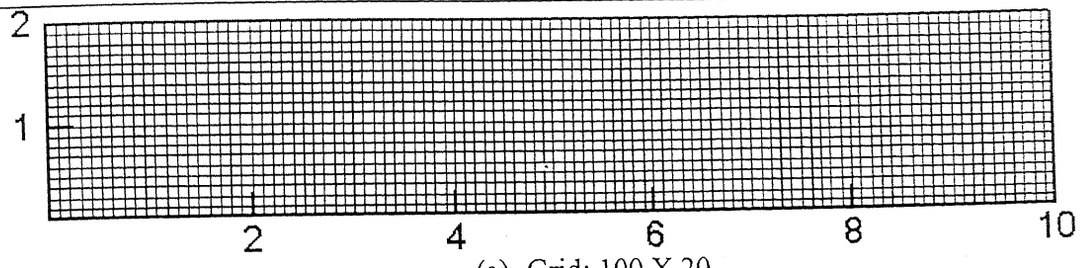

(a) Grid: 100 X 20

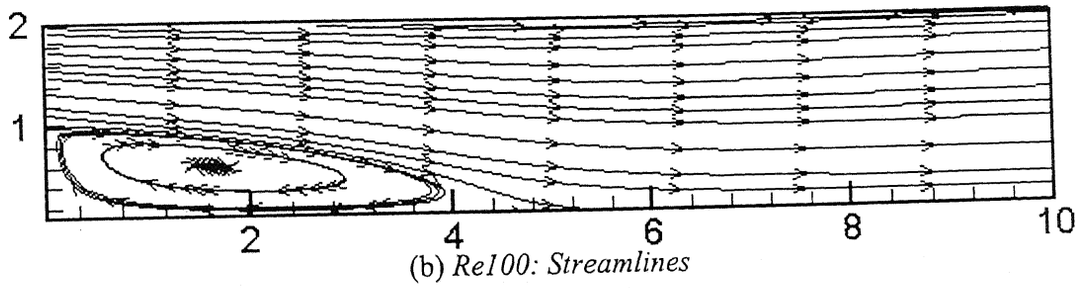

(b) *Re100: Streamlines*

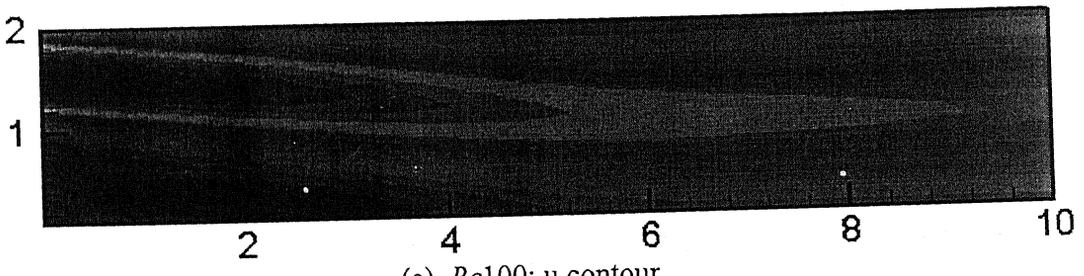

(c) *Re*100: u contour

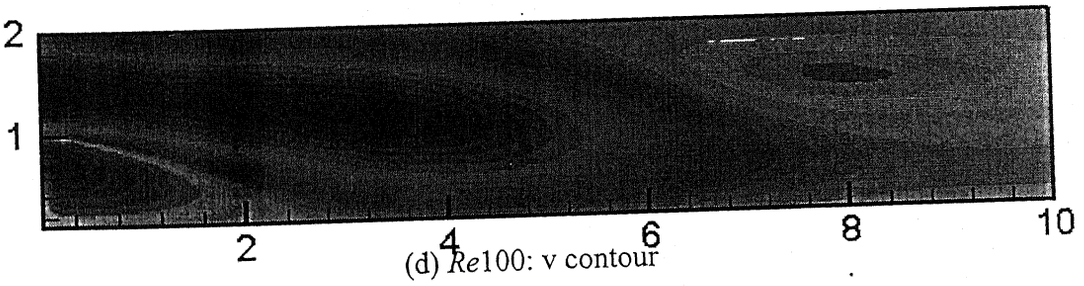

(d) *Re*100: v contour

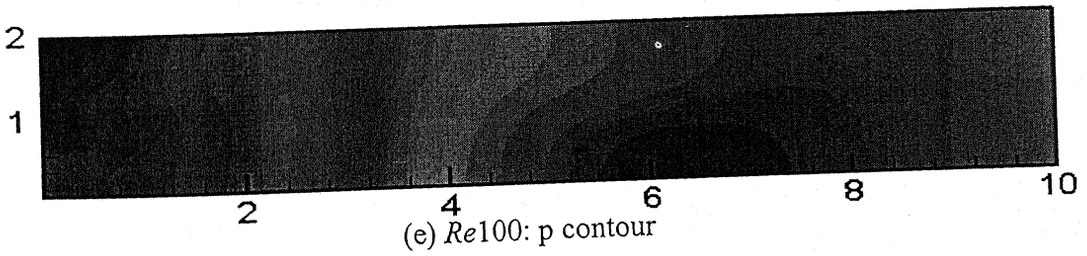

(e) *Re*100: p contour

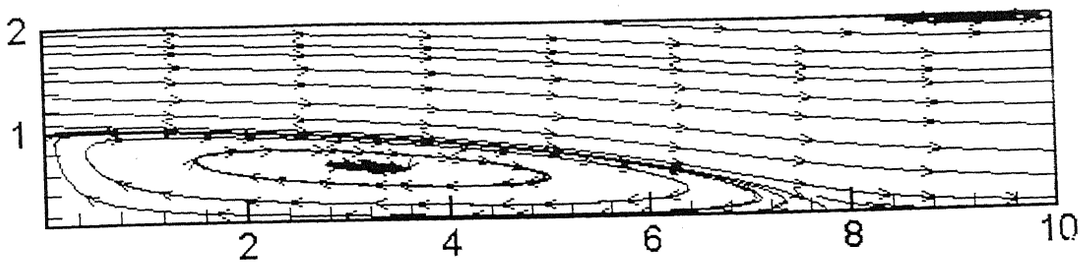

(f) *Re*200: Streamlines

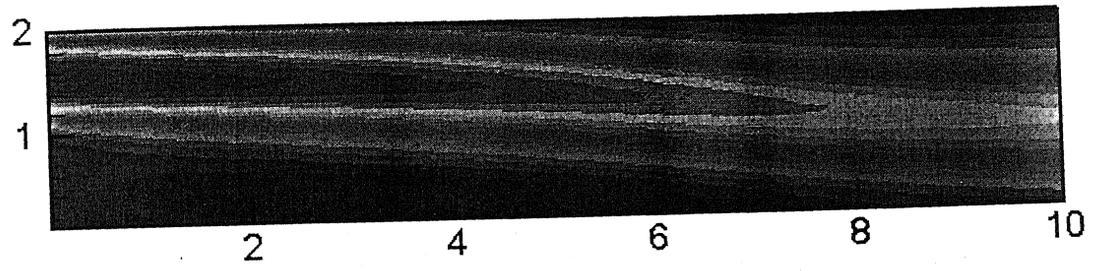

(g) *Re*200: u contour

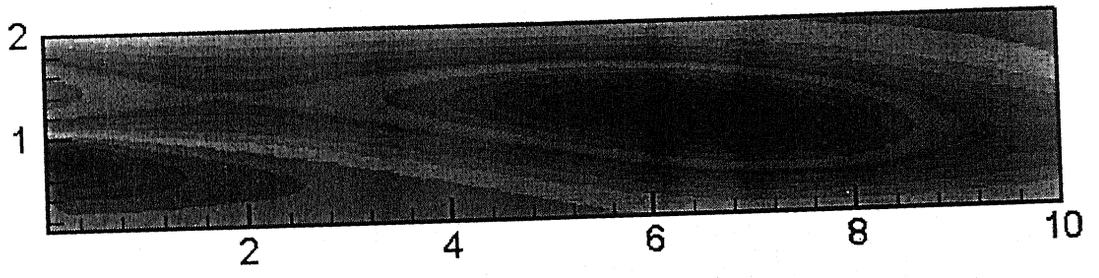

(h) *Re*200: v contour

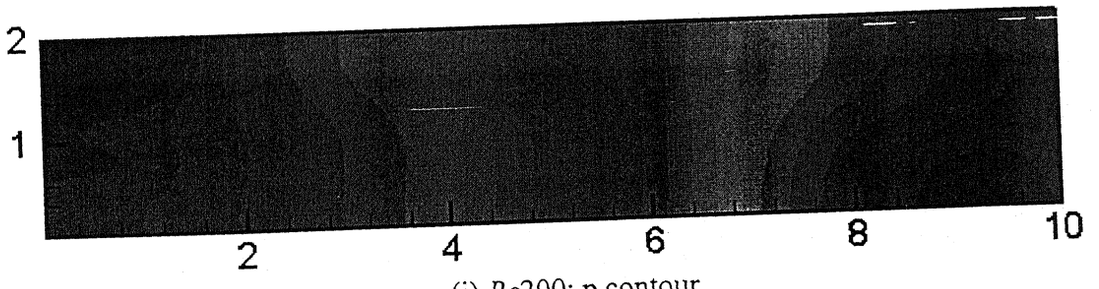

(i) *Re*200: p contour

Figure13: a-e plots for *Re100* over a backward facing step
f-i plots for *Re200* over a backward facing step

The above plots are for demonstrating the variation in the reattachment length on varying Reynolds number and showing qualitatively the distribution of u, v and p values on such kind of a flow.

Computational Results

Unsteady computations were performed in a 50X10 mesh. The problem was solved in a non-inertial grid by adding sinusoidally varying acceleration of the frame to the v-momentum equation a outlined in the paragraph on extended Galilean invariance. The effect of oscillation was very obvious, as pointed out in the following contour plots, one without any acceleration of the frame and the other with acceleration of the frame.

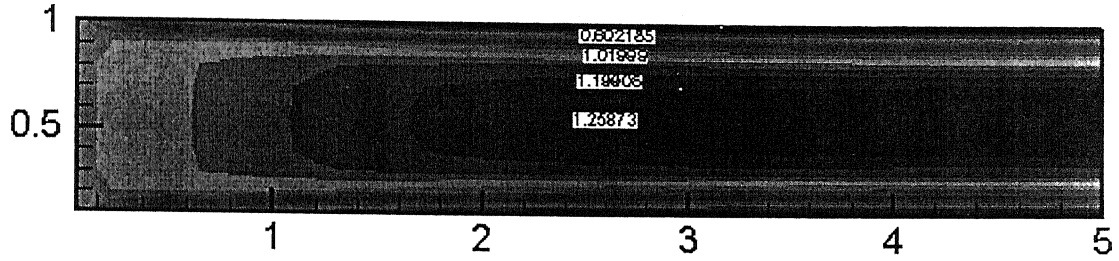

u contour, *Re* 500

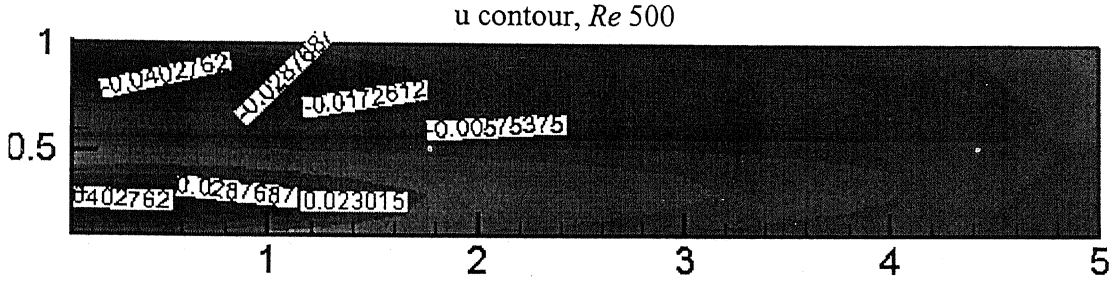

v contour

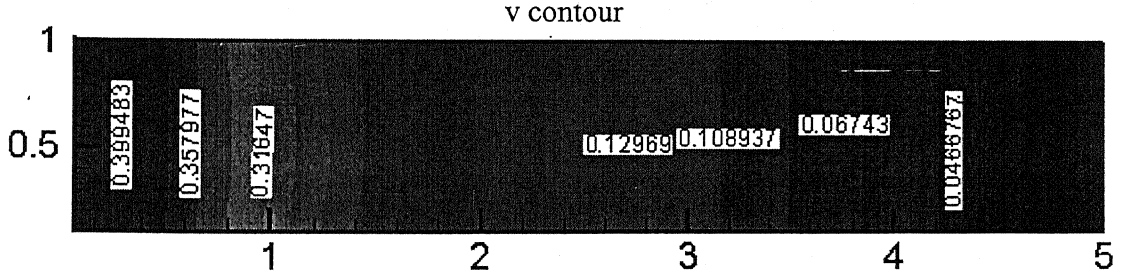

p contour

Figure14: Contour plots in a channel without acceleration

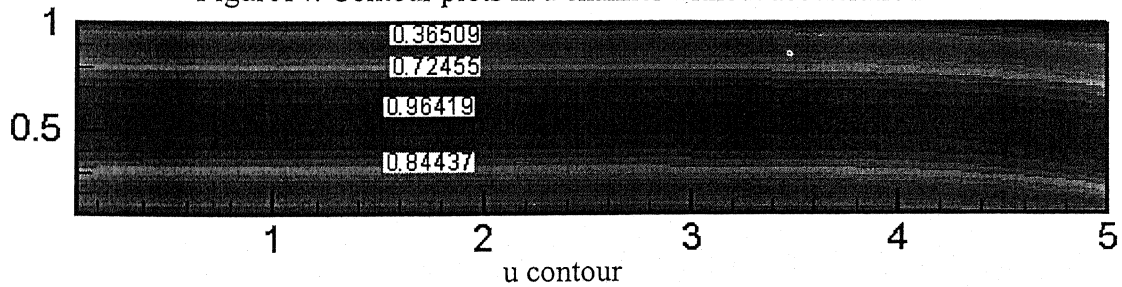

u contour

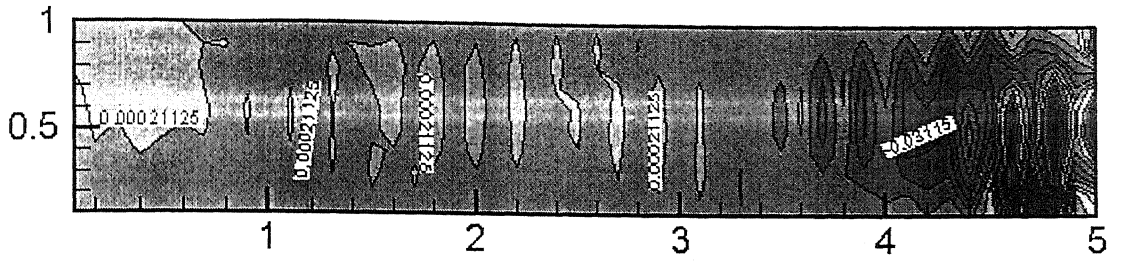

v contour

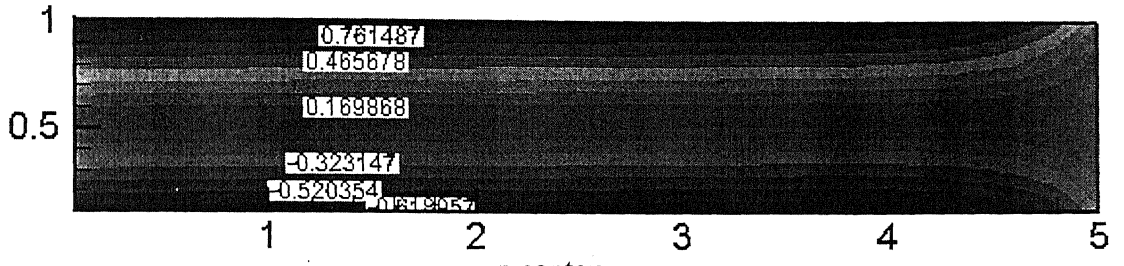

p contour

Figure15: Contour plots in a channel with transverse acceleration

Now, there is observed periodic reversal of the high and low pressure zones as the computation progresses as shown below.

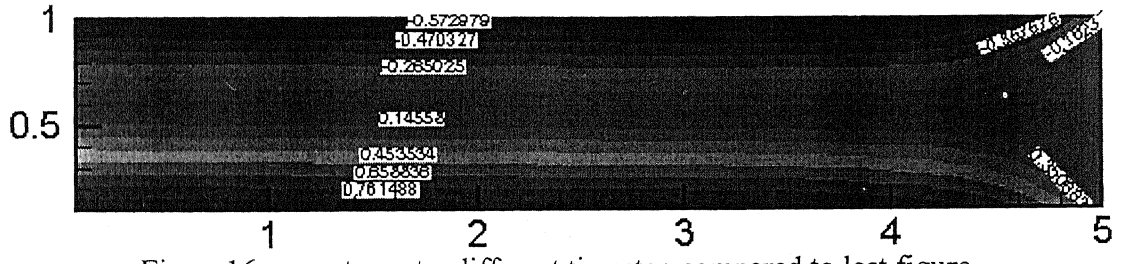

Figure16: p contour at a different timestep compared to last figure

This reversal of the pressure zones was seen to be exactly following the frequency of oscillation. The following plots of pressure values at the beginning, 2-d, 4-d and exit when oscillation frequency was 1 Hz. The same trend was spotted at other frequencies.

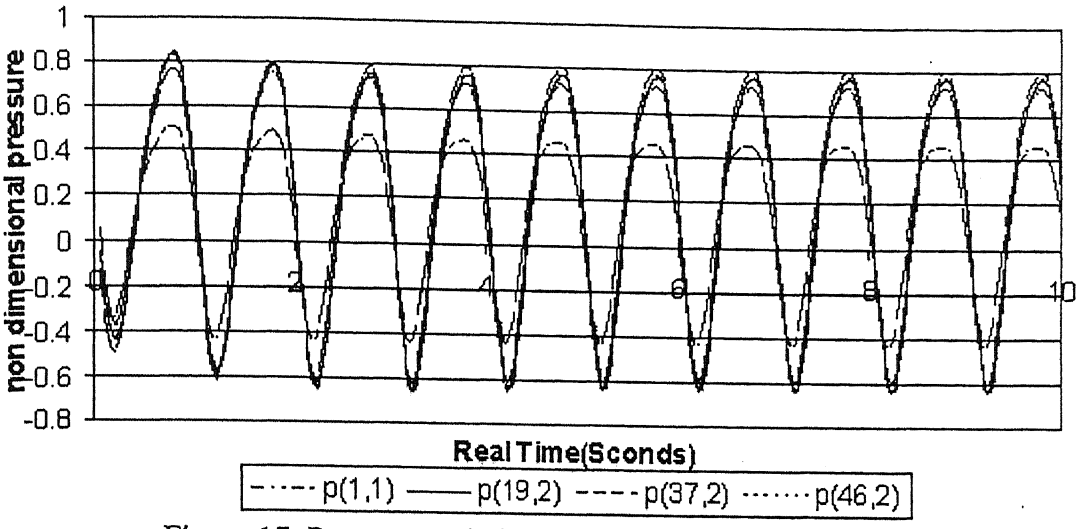

Figure 17: Pressure variation along the axis of the channel

The following variation in velocity were seen at a location (49,7). at the exit.

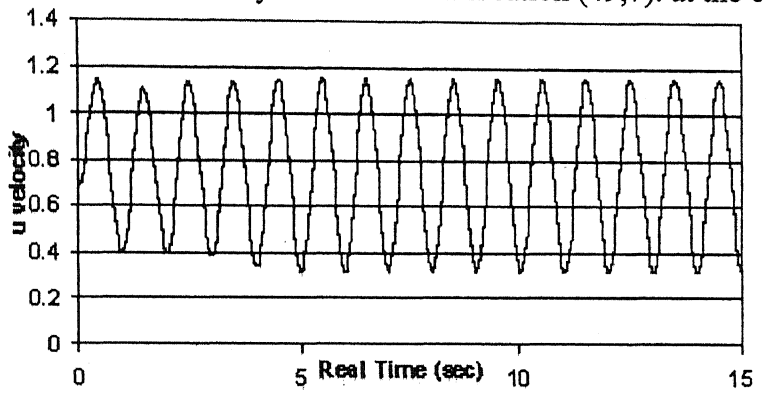

The u velocity was increasing at the beginning in mean value but became steady after about 5 seconds. The u velocity was seen to have a phase lag compared to pressure oscillations as shown below.

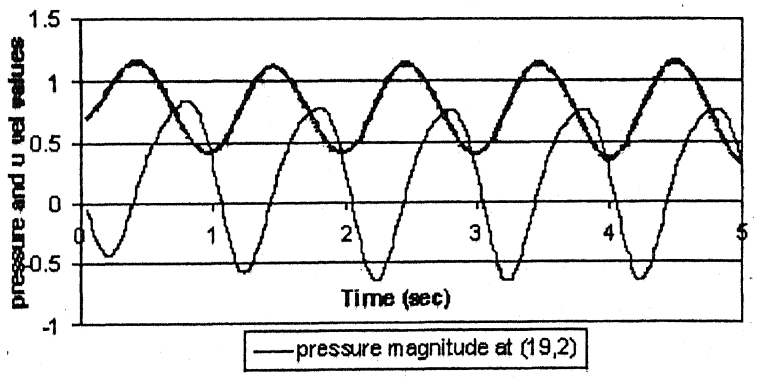

At the exit, u velocity is seen to reverse directions at the corners such that vortex formation and shedding takes place. The frequency of such shedding was same as oscillation frequency and the size of the vortices were seen to increase with frequency

of oscillation and a decrease with increasing average velocity of the axial velocity. The domain reached steady state finally in all oscillation frequency cases.

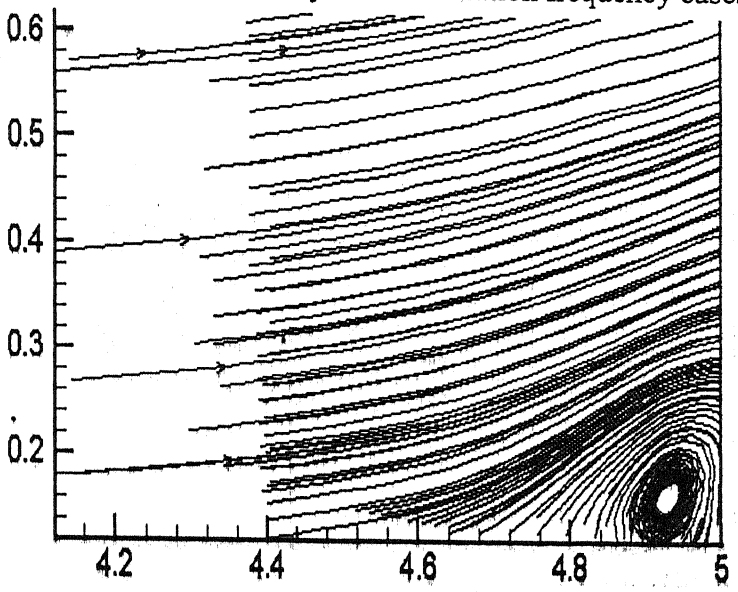

Figure18: Formation of vortices at the exit

The u velocity vectors responsible for the formation of eddies at the outlet show limit cycle behaviour at higher frequencies. The following are the plots of u velocity magnitudes at various axial locations for different times during one cycle and the numbers in the plots indicate i index of a location. It is seen that the u velocity profile at the exit remains almost same all through the time period except when it reaches an average profile during change of pipe traverse direction. But the important thing is that the asymmetry of the profile does not change, unlike in a lower frequency situation like 8Hz case where there is periodic reversal of the location of maximum velocity. That would indicate that the u velocity low value and high value regions remain somewhat concentrated at the same locations when the frequency of oscillation is large and oscillates periodically (i.e. more capable to adjust to the flow domain movement) at lower frequencies. So, the vortices formed at lower frequency will be oscillating about the central line but in the higher frequency case, it will remain somewhat fixated.

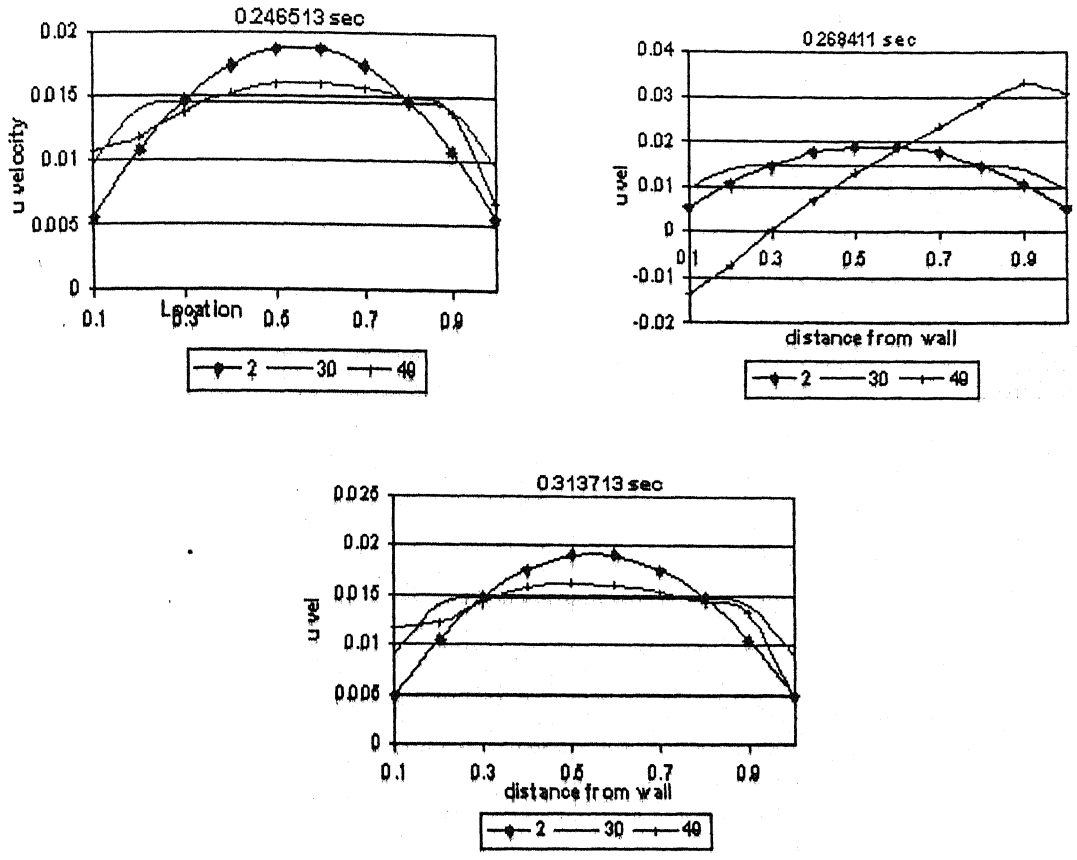

Figure19: u velocity profiles at three axial locations at frequency 16 Hz during a cycle

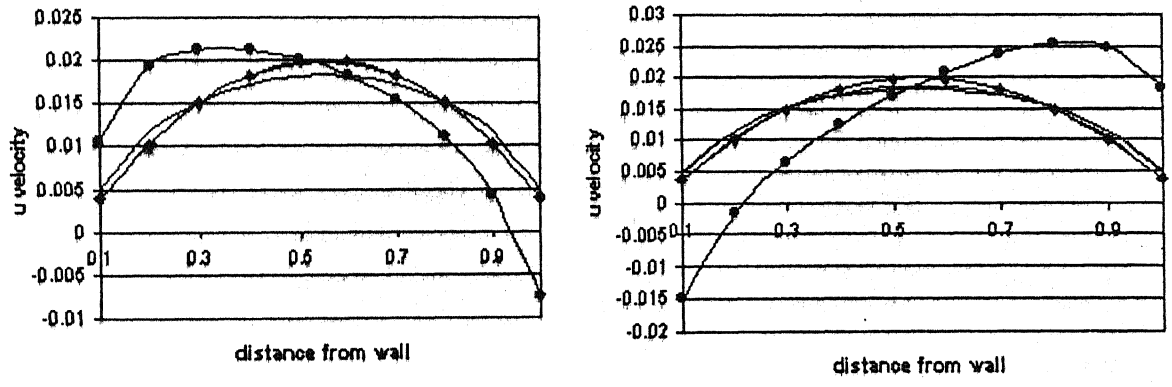

Figure20: u velocity profiles at same three axial locations at frequency 8 Hz during a cycle

The following were two very independent findings from the numerical results:

- Pressure fluctuation (max-min) increases with both amplitude and frequency of oscillation
- Mean values of pressure drops with both amplitude and frequency of oscillation!!

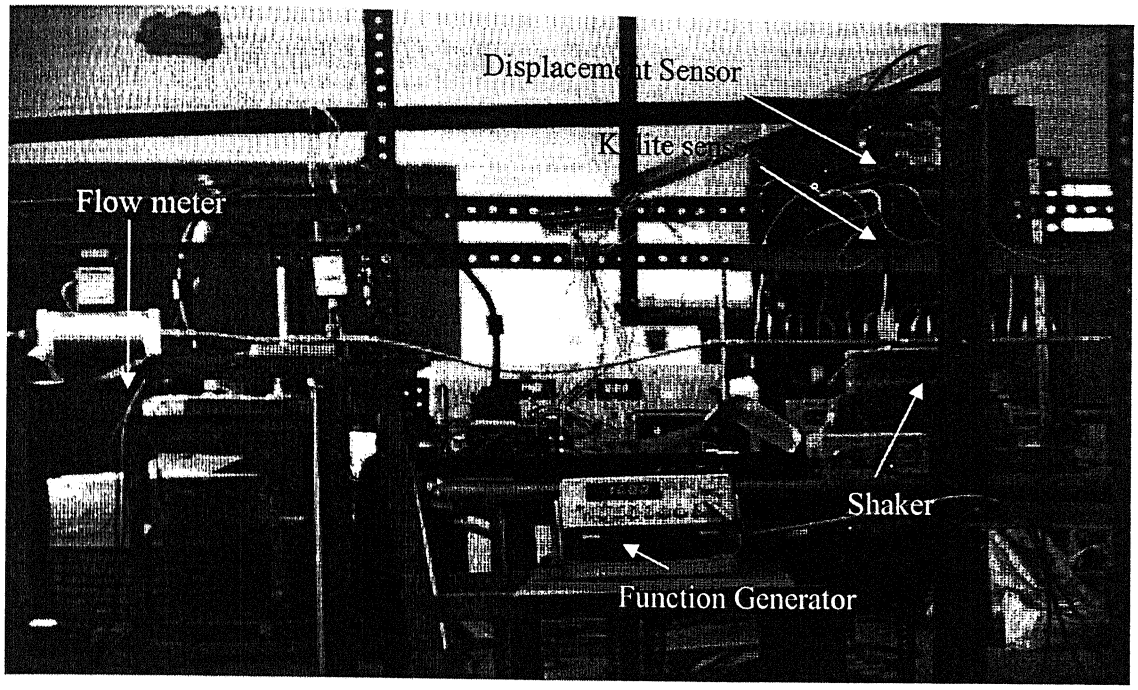

Figure21: Experimental Set up Photo

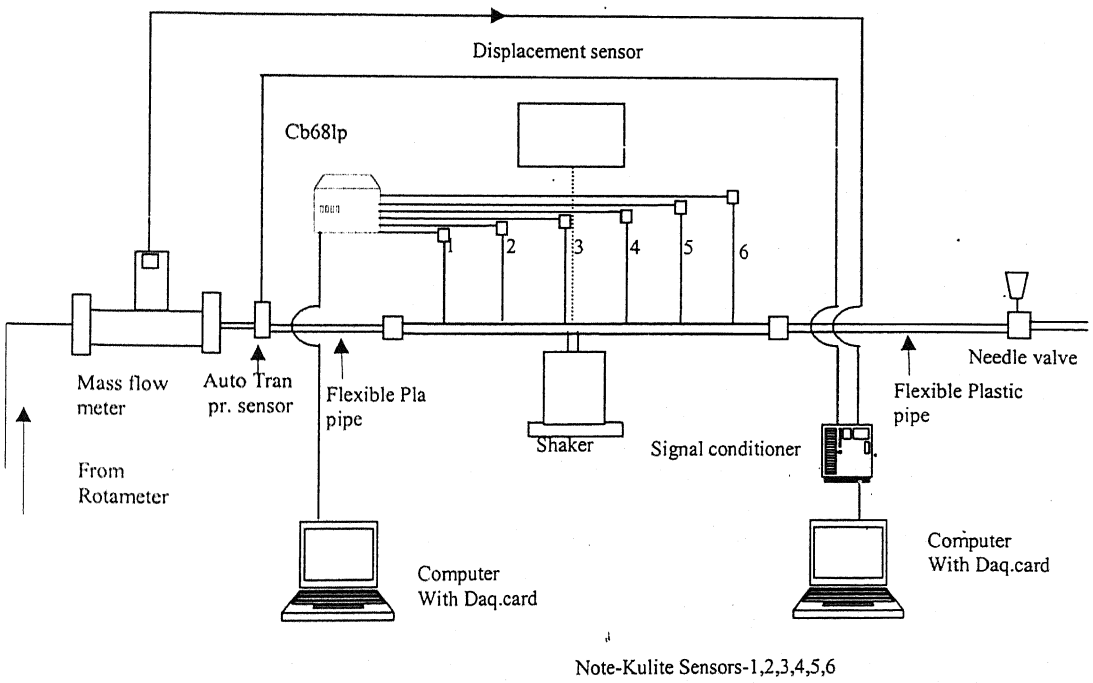

Figure22: Experimental Set up Sketch

A schematic illustration of the experimental setup is shown in Fig.15. Compressed air, at known and regulated pressure was introduced into the pipeline

through a calibrated rotameter that measured the flow rate of the air. The Reynolds number of the incoming flow was changed over a range by varying the air supply pressure and the air flow rate. The air supply pressure was varied using a pressure-regulating valve and corresponding to each supply pressure, the airflow rate was varied over a range using a needle valve located after the rotameter. The volume flow rate was then measured accurately using a thermal flow meter, which was first calibrated first against known supplies and a voltage-flow rate calibration curve could be arrived at. Just before entry to the pipe examination section through flexible plastic tubing, a robust Auto Tran model 860 transducer based pressure sensor was placed. The purpose of usage of this sensor was to have knowledge of the pressure in the line before flow enters the main pipe section, so that any sensitive sensor downstream could be protected. , Six calibrated piezo-resistive highly sensitive Kulite pressure sensors (Model XCS 50-D) were used to measure the wall static pressure uniformly at six locations along the length of the pipe. The maximum frequency ranges of the sensors were 10 kHz. The kulite pressure sensors were connected to the pipe through flexible rubber tubings of small lengths, so that they can be protected against vibration of the pipe from being transmitted to it. The sensors are highly sensitive to vibration and they pick up minutest of pressure variations going around in the surroundings. The pipe was clamped in the middle to an electromagnetic shaker for which the power amplification circuit was designed in-house. The displacement of the pipe during oscillation was measured using a laser based Keyence displacement sensor. The input to the displacement shaker was given using a highly accurate function generator. The flow sensor and the inlet Auto Tran pressure sensor were connected to a different PC via a National Instruments signal conditioning board. The kulite sensors and the displacement sensors were connected to the PC through a CB68-LP connecting block.

In each PC the data were acquired using an eight channel, 16 bit NI DAQ card into a computer using Lab VIEW data acquisition program. The data from all the sensors were acquired simultaneously, without multiplexing, with a typical scan rate of 200 samples/second for 10 seconds to capture all possible ranges of frequencies that might be present in the pressure oscillations. The stored data were processed using MATLAB on a personal computer. The pipe in the study was a milt steel tube of 12mm outer diameter, 9mm inner diameter and 500 mm length. The sensors were connected to the pipe through flexible tubings and pinholes, which were placed on the pipe at distances from the inlet of $3D_{in}$ (port 1), $13D_{in}$(port 2), $23D_{in}$(port 3), $33D_{in}$(port 4), $43D_{in}$(port 5), $53D_{in}$(port 6).

Experimental Results and Discussion

The results obtained in the numerical simulation is of some theoretical importance in the sense that they predict the behaviour of the system under the most ideal of situations, with the limitations imposed by the treatment of the boundary conditions and other things regarding the implementation of the numerical schemes for solving the full Navier Stokes equations, but they fail in general to capture the complex dynamics of the flow situation actually taking place as is revealed by the detailed experimentation. The most serious deviations possibly occur in the computations because of the implementation of the pressure boundary condition. As in SMAC, the pressure boundary condition is not applied (its only pressure correction boundary condition that is applied). However, in real life flows through closed conduits, it's the distribution of the pressure filed that governs the flow and hence the treatment of the pressure boundary condition is of utmost importance to capture the true flow dynamics. For that reason, in the present study, the investigation of the changes in the pressure field is the central focus.

The experimental results capture the flow situation in exact and far more extensive details because of some very apparent reasons. They include the following:

1. The real flow is taking place at Re>4500 with air as the fluid, so the flow is turbulent. The solver has been prepared for laminar flow conditions of the flowing fluid. However, with a level of mass flow in the ranges of 30grams per second and water as the liquid, with the dimensions of the conduit kept constant, the flow Reynolds number would correspond to a realistic flow rate like that in an engine supply of HPT-32 training aircraft of the Indian army, hence the

results are in fact derived for a different situation compared to the one carried out in the experiments.

2. As mentioned above, the treatment of the pressure boundary condition has a significant effect on the computation.
3. There would be complex interaction between the flow just coming out of the inlet and the flow slightly downstream of it. In a real situation of water flowing through the pipe, the flow slightly downstream will have on it very pronounced effect of vibration. This complex phenomena of interaction between the incoming fluid as it enters the oscillating domain and the flow situation existing inside has a pronounced effect on the flow upstream and thereby effects the flow that is being discharged on the outlet of the conduit (into the combustor in some real cases!). An effort has been made to show the variation clearly.
4. The geometry of the conduit will not be as perfect in the real case. That will have some effect on the flow through it. Also, the attached components of the set up, like the inlet pipe that delivers the flow but does not have the exactly same motion as the oscillating pipe being studied, the tappings used for using the pressure probes etc, will have effects on the flow as well and that will not be reflected in he computational results.

While looking at the results of experiments in general, it is very important to keep in perspective the results obtained in the no-oscillation case. The results of the no-oscillation case serves two very important purposes, namely, providing the basis for comparing the results obtained in the cases with oscillations and pointing out the importance that inherent structural properties of the pipe will have in dictating the

results as obtained with oscillations of the pipe. The figure below(figure1) shows the general distribution of pressure across the various pressure scanning ports (used for the sensing of pressure by kulite piezo-resistive type sensors) along the length of the pipe.

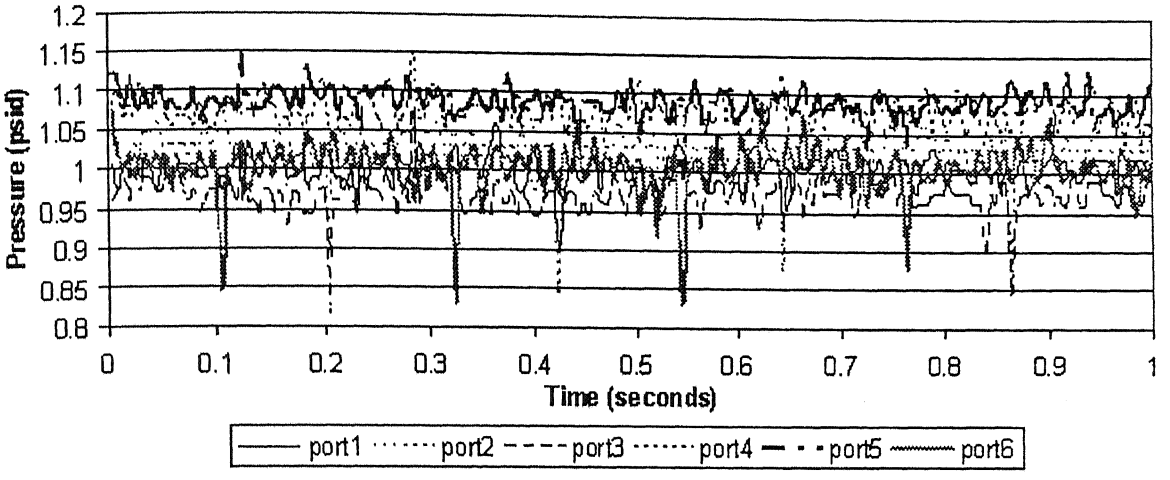

Figure23: Pressure distribution with no oscillation

The above pressure distribution shows up a very interesting phenomenon. Though in general, there is not much variation in the average values of the pressures noted at various ports, there are drops taking place at every location with comparable frequency. The observation is augmented by an fft analysis of the oscillating component of the pressure data done on MATLAB. In the plotting of the fft spectrum, an averaging has been done over 5 points to represent the absolute value of the fft at the midlocation of those 5 points. The plot of the same is given below in figure2.

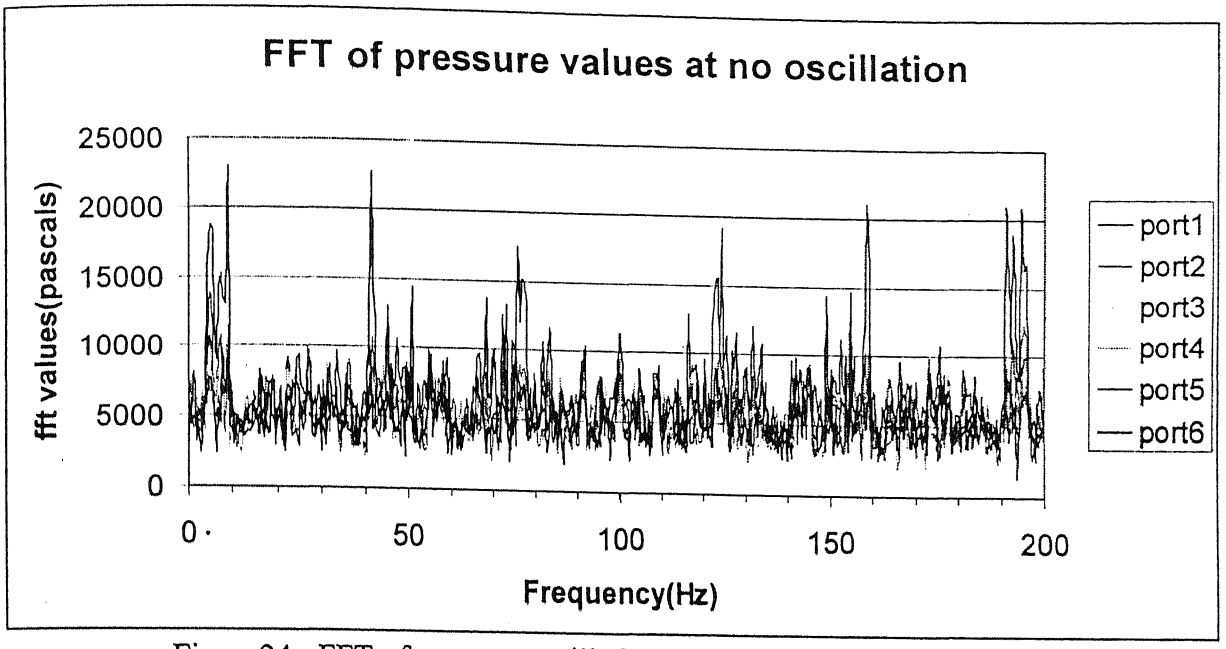

Figure24: FFT of pressure oscillations at no pipe-oscillation

There are a couple of features that are very prominent from the above figure. Firstly, the peaks occurring for the pressure values of the port6 are above the peaks of every other ports, which indicates larger values of oscillating component for the port6, even though a plot of the pressure values at any time instant along the length of the pipe shows(Figure3) that the maximum values of pressure is occurring at port 5.

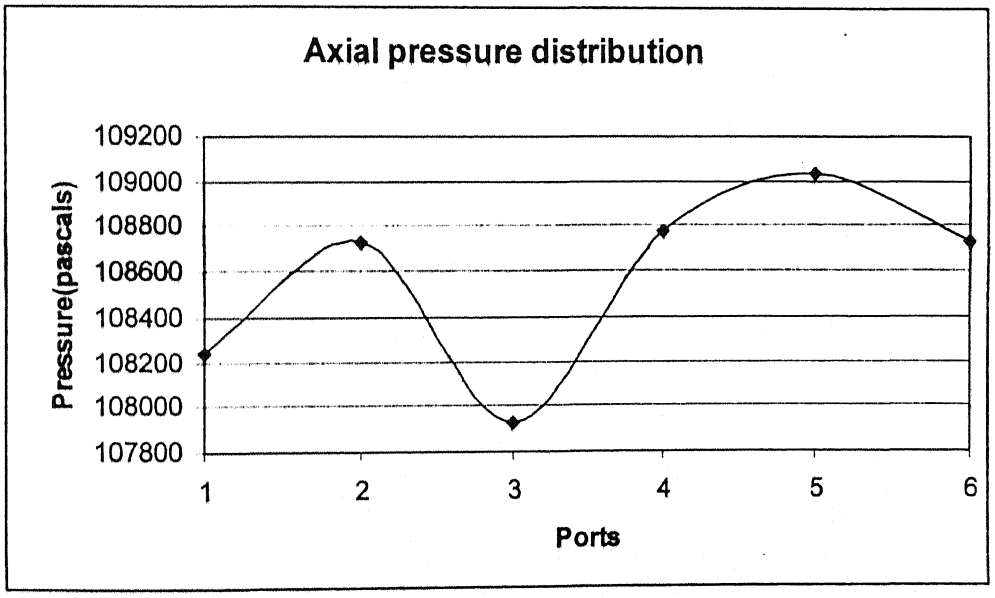

Figure25: Axial pressure distribution for the pipe without oscillations

The other very important feature that can be observed from the fft plots is the spectral distribution of the peaks. The largest peak for port no 6 is

occurring at a frequency of 8.75 Hz and another major for port 6 is occurring at around 41.25 Hz which can be considered as a harmonic of the previous. Other than that we observe peaks around 46 Hz and then another at around 75 Hz. The ffts were done upto 200 Hz with folding occurring at 100 Hz, so we don't look beyond 100 Hz for peaks. The peaks for other ports are also seen to be clustered around those above mentioned values. Since there is no oscillation taking place in the pipe with flow through it at 20 litres per minute, one would tend to think that they must be reflecting the inherent structural behavior of the pipe. A determination of fundamental frequency of the pipe with the dimension as outlined in the experimental set up descriptions, indeed reveals that they(i.e. frequencies at which peaks are occurring in the above figure) are the values reflecting the first few modes of vibration of the pipe(assuming a free-free boundary condition)and the their harmonics at times. The figures below indicate the mode shape analysis figures as obtained using ANSYS. The absence of aliasing present in the data is also evident from the fact that the expected system behavior is starkly evident and the occurrence of higher frequency oscillations aliasing as lower frequency is also not there because the system behavior has only lower frequencies associated with them and they are highly visible, not contaminated. These results therefore show that the scan rate of 200 Hz is apt for the given system here.

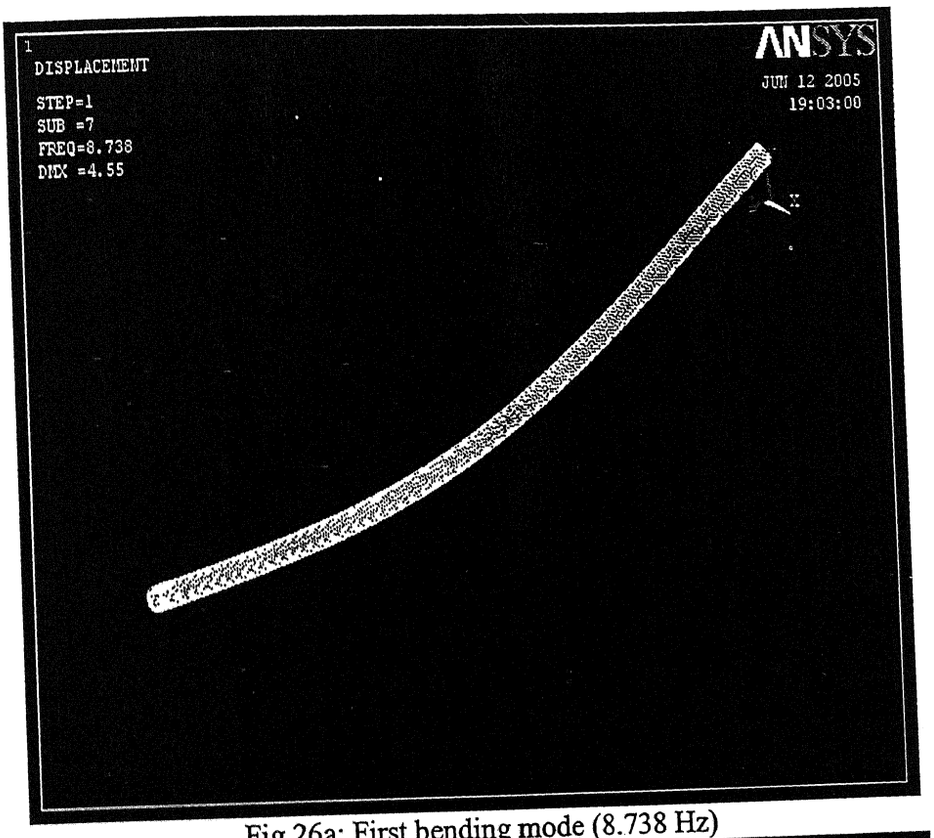

Fig 26a: First bending mode (8.738 Hz)

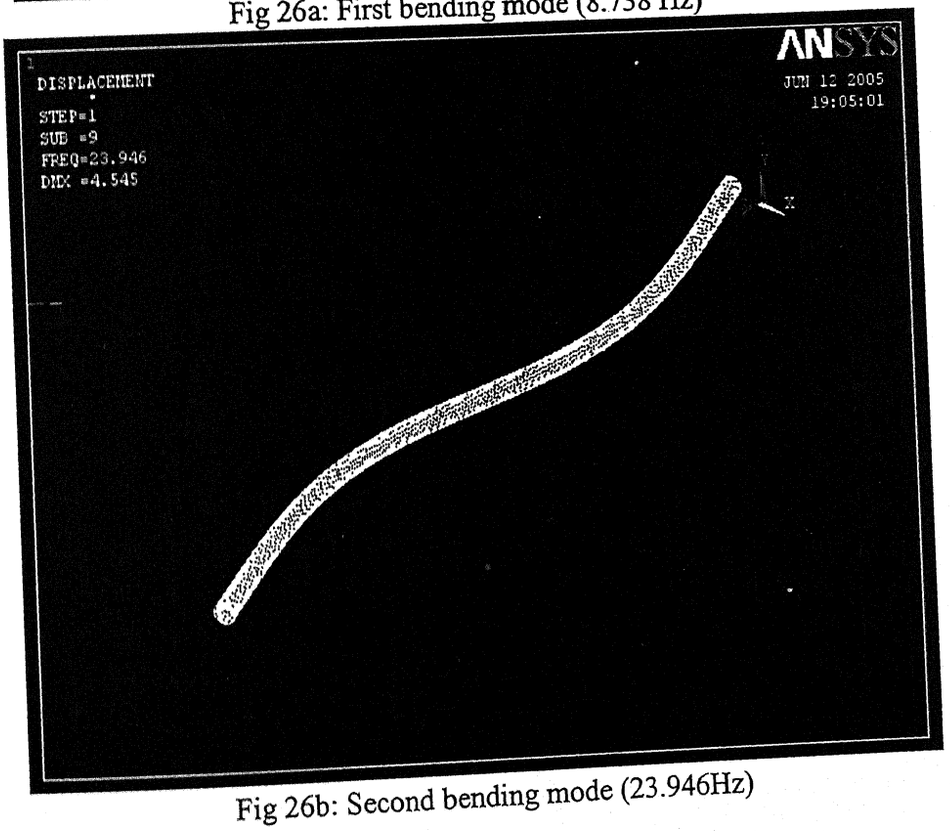

Fig 26b: Second bending mode (23.946Hz)

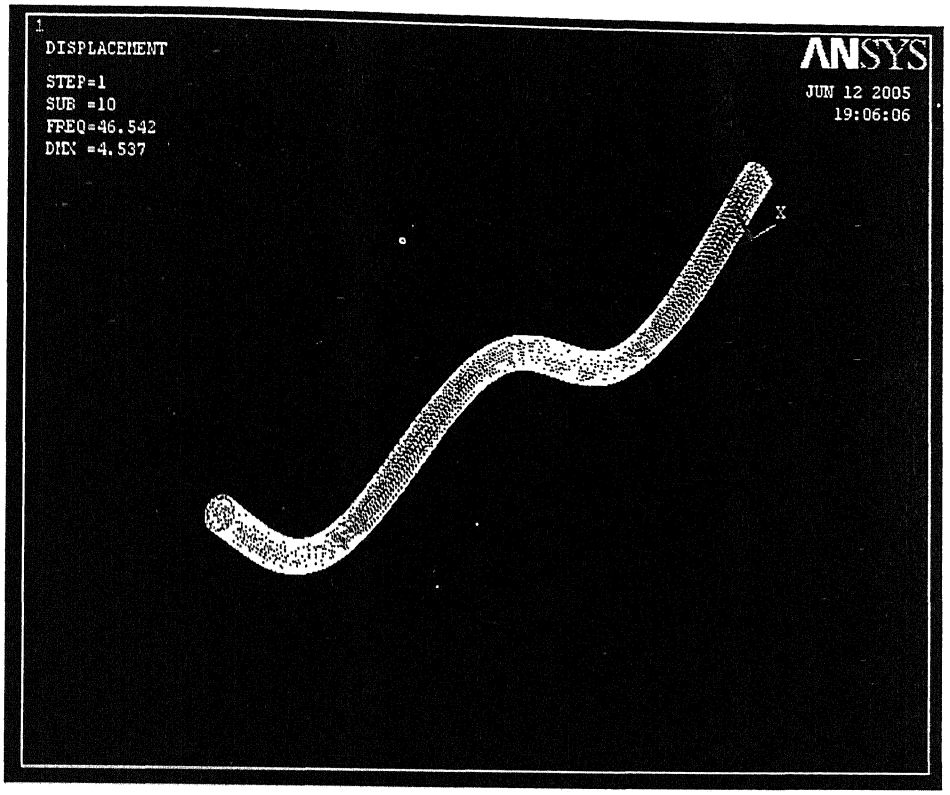

Fig 26c: Third bending mode (46.542 Hz)

Now one can have a general look at the pressure data obtained during the time when the pipe was oscillated at regulated frequencies and amplitudes. The mild steel pipe was given oscillations at frequencies of values ranging from 4Hz through 32 Hz, including both the values, in steps of 4Hz. These variations in frequencies were carried out under fixed values of amplitudes of oscillations of magnitudes starting from values of 4 through 12 in steps of 2, as shown on the signal generator. The displacements were tracked using a calibrated laser based displacement sensor from Keyence, the description of which was given in the "experimental setup" portion. The values of the displacement as obtained from the shaker where not perfectly consistent and the measures obtained were somewhat contaminated with the noise that was being picked up by the displacement sensor from the surroundings (e.g. noise produced by the movement of personnel in the lab etc), but a general quantification of the displacement could be done as follows:

Indicative Displacement	Actual Vertical Traverse (twice of amplitude of motion)
Amp1	1.40mm($0.155D_{in}$)
Amp2	1.55mm($0.172\ D_{in}$)
Amp3	1.70mm($0.188\ D_{in}$)
Amp4	1.85mm($0.205\ D_{in}$)
Amp5	2.00mm($0.222D_{in}$)

Now we can discuss about some general observational features of the pressure distribution obtained on oscillating the pipe at various frequencies and amplitudes.

First let us consider a general distribution of pressures at various ports at frequency 4. It will be shown later using spectral distribution of oscillating component magnitudes of pressure that the maximum amount of oscillation takes place at port3 and at port6. And of them, it can be easily observed that even though the average value of pressure is almost all the cases minimum at location 3, the drops at locations 6 often rival them in magnitude. Let us take a representative distribution at pipe-oscillation frequency of 4.

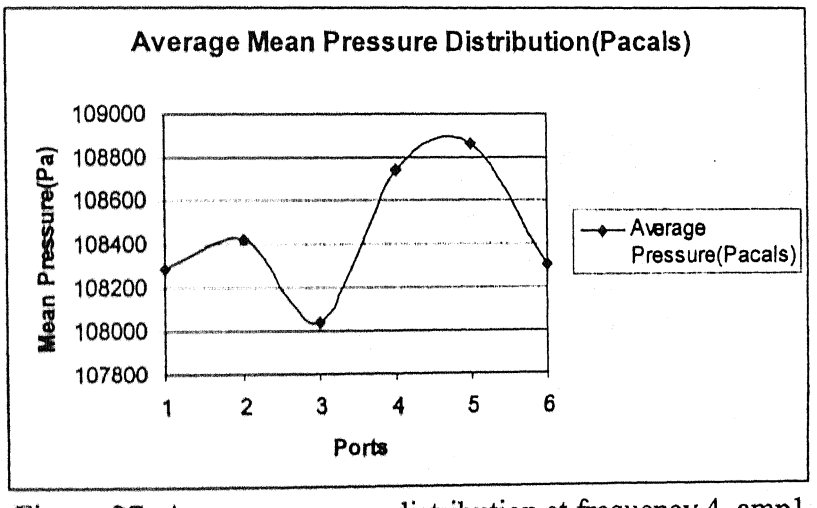

Figure 27: Average pressure distribution at frequency 4, amp1

Now comparing the pressure values at ports 3 and 6 at frequency4 and various amplitudes:

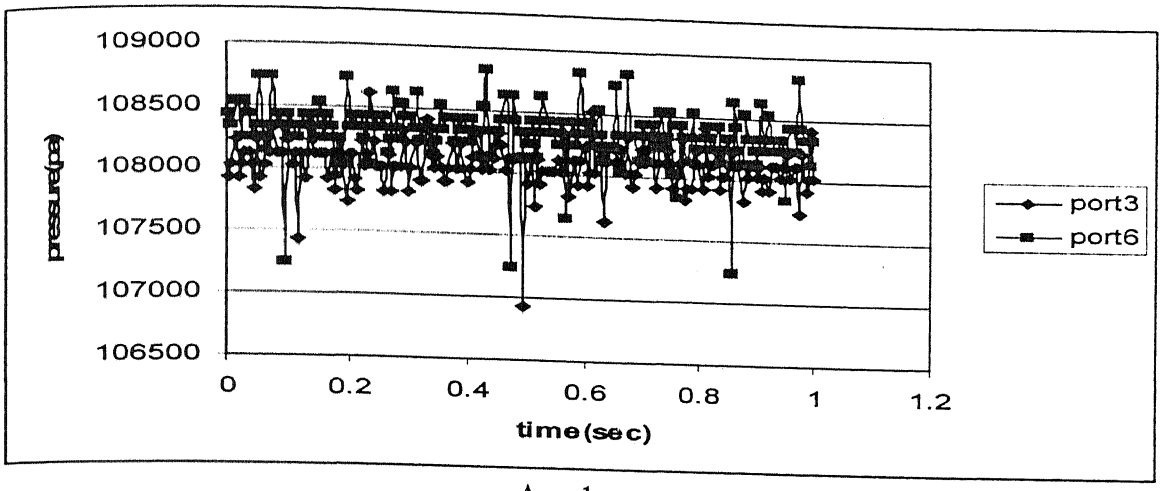

Amp1

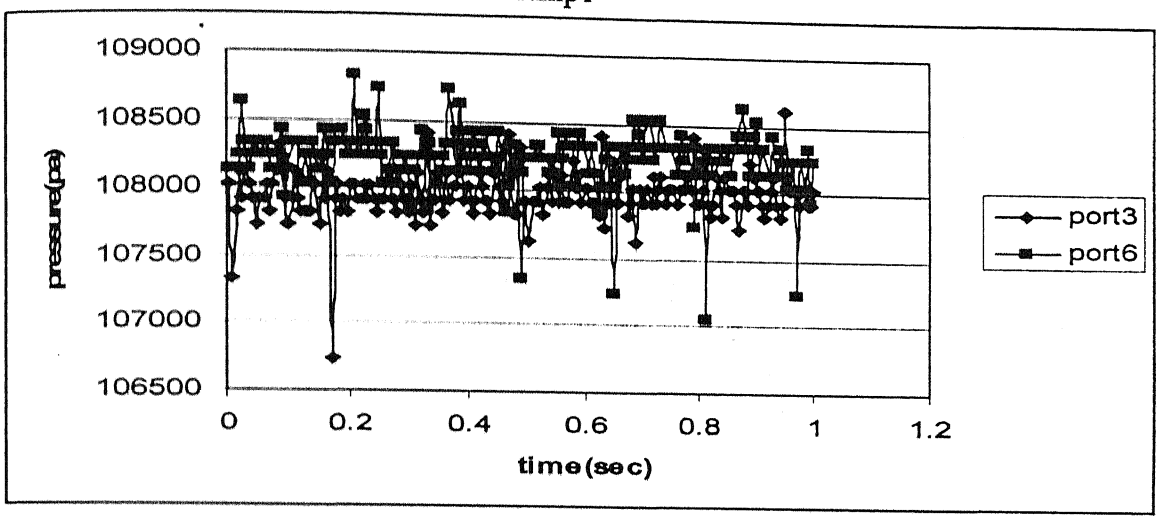

Amp2

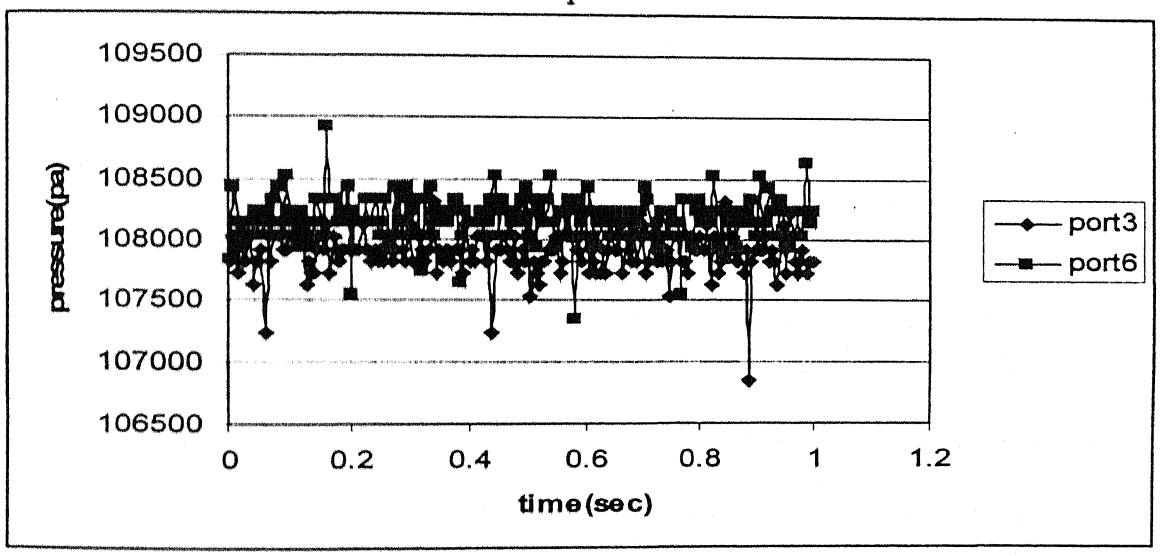

Amp3

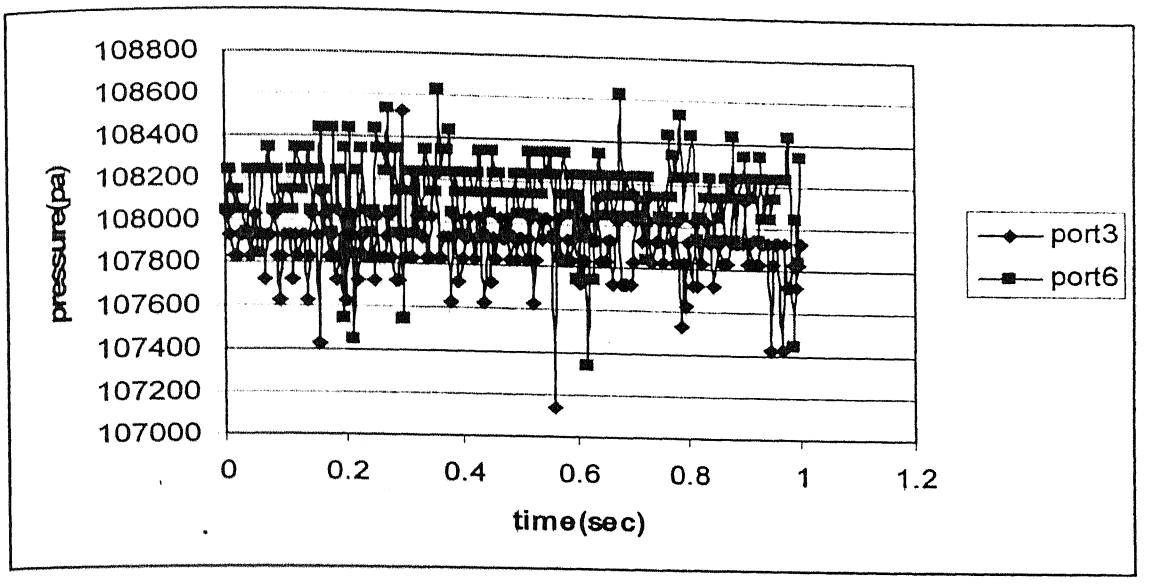

Amp4

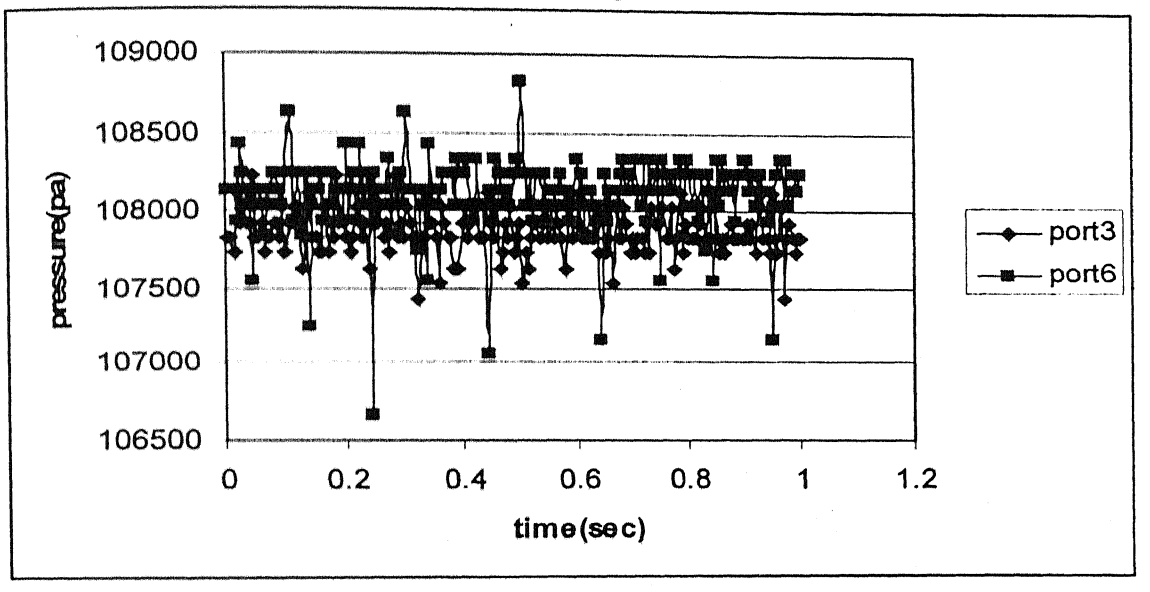

Amp5

Figure 28: Pressure values at ports 3 and 6 at frequency4 and various amplitudes

The above plots show a few general tendencies in the pressure drop patterns. Firstly, at lower frequencies, the frequencies of pressure drops are fairly comparable for both the ports; however, as the amplitude increases the frequency as well as the magnitude of drop at the sixth location becomes more prominent, even as the difference of average values increases. Secondly, there can be seen a drop in the average values of the pressures with increase in amplitude. Both of the phenomena can be explained if one considers the overall fluid dynamical and structural effects that are present in the flow as follows.

The phenomena occurring inside the flow field shows the effects of the following properties of the fluid at large, namely, the inertia and compressibility of the fluid medium and the turbulence existing in the flow due to high velocity of the fluid flowing. Depending on the boundary condition at any given moment, the effect of one supersedes the other and thus the behaviour shown in the plots are manifested. For example, consider the moment when the pipe starts moving upwards. The fluid layer immediately in contact with the lower half of the pipe wall will have the maximum tendency to move and there would be created a vacuum like situation at the top/diametrically opposite side of the wall (the same effects will be played cyclically continuously at both end). The tendency to move will impart both an axial and transverse (along the line of motion of the pipe) momentum to the fluid inside. Now the transverse momentum has more obstacles against it because there is significantly less room available in the diametrical direction for the movement. So, it leads to the fluid getting compressed and thus arises the effects of compressibility. This component also has the effect of damping out the pressure oscillations. Whereas, the axial momentum has more room for it to maintain itself with varying degrees of difficulty depending on the position along the axis and hence the nearby boundary condition (like whether this is the direction from where flow is coming in or this is the direction in which the fluid is escaping the pipe into another pipe of zero gauge pressure). Depending on which effect has more predominant role to play at a given moment for a fluid particle, the compressibility effect will raise the pressure in general and the inertia effect will try to lower the pressure in general (under many cases, the inertia will add to the compressibility as well). Added to that effect is the structural effect of how much actual displacement is actually taking place at any axial location of the pipe. Through fft data plots at various frequencies, it can be seen later

that the harmonics of the first and thirds modes of vibration of the pipe are more prominent in the pressure drops. The mode shapes indicates that the ends of the pipes will have the maximum displacement from the midpoint of the pipe compared to the other locations of the pipe. But the pipe inlet is more rigidly fixed to the surrounding structures in the experimental set up, so it has lesser of a chance to move and hence the outflow end will have the maximum displacement. Therefore, the cyclical effects of compressibility and momentum transport will have more impact on it and it will have more fluctuations in its values. On the other hand, the fluid particles towards the inlet will have to move against the incoming flow which will try to damp out most of the flow fluctuations taking place in there. The effect of the incoming flow can also be seen when comparing the pressure fluctuations taking place at any other frequency and amplitude in that there is comparatively lesser amount of oscillations taking place at most of the port readings compared to the oscillations observed during the zero readings (figure1). This again can be attributed to the dissipative effects of the turbulence presence in the flow (the parameters of which are not subject of the study being done here). So, the overall nature of the pressure distributions captured is basically result of the interplay of these three effects, namely, inertia, compressibility and turbulence present in the flow. Most of the features seen in the experiment can be explained considering the comparative effects of the three above effects.

When one tries to intuitively predict the maximum frequency present in the pressure fluctuations, it seems logical to think that the maximum frequency present must not be above a few harmonics of the, say, third mode of vibration of the pipe because frequencies beyond that will be damped out by turbulence present in the flow as well as due to the fact that vibration of the pipe has a damping effect on the

flow and also the high values would be really difficult to characterize as to what is the cause of their origin, the oscillation of the flow domain or the turbulence itself.

Now, let us have a look at the fft plots of the oscillating components of pressure on port 6 at various frequencies and amplitude Amp5 (pipe traverse 2mm).

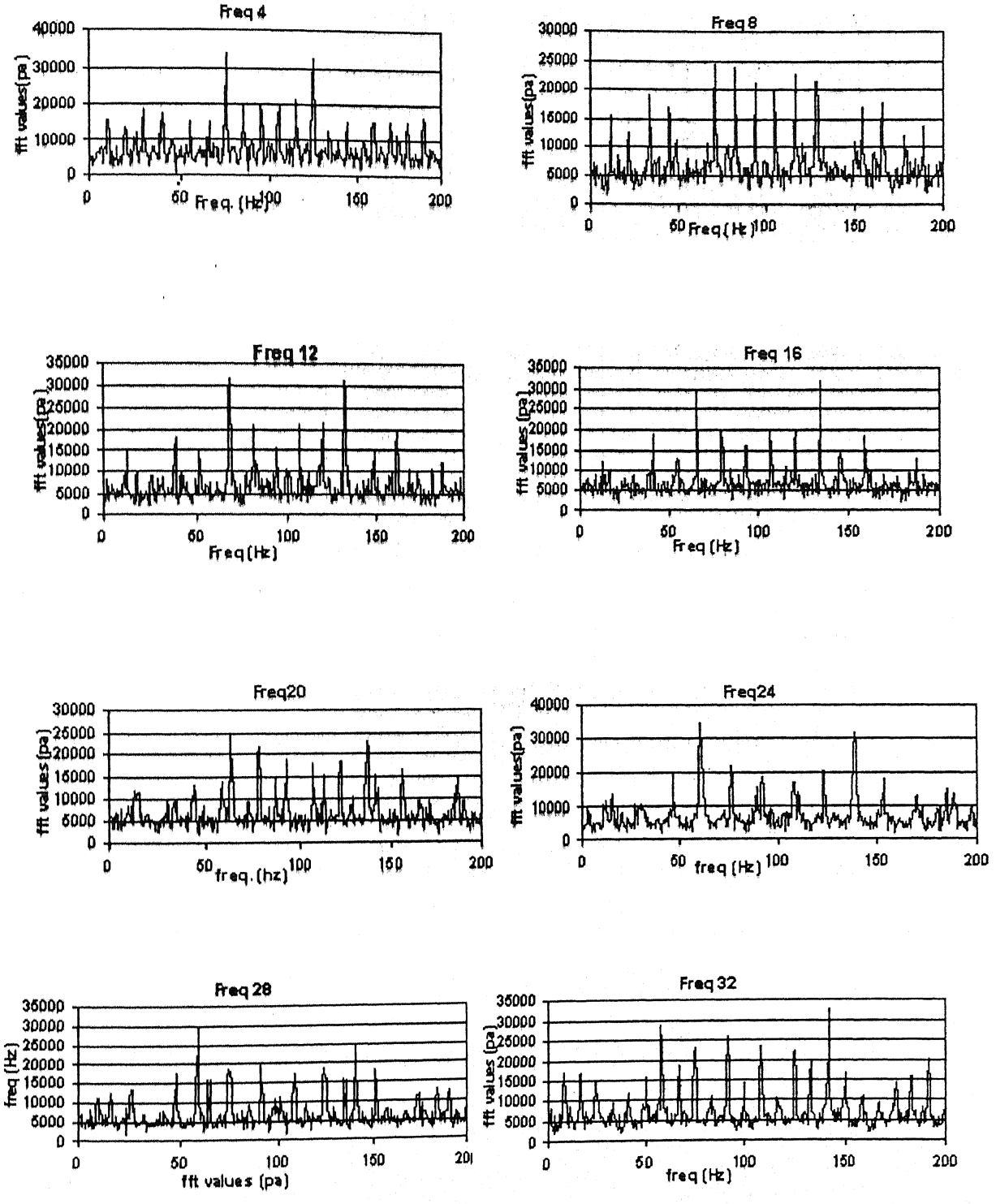

Figure29: FFT analysis plots at Amp5

The above plots point out a few very important characteristics of the system.

Firstly, it is very evident that the pressure oscillations are very sensitive to pipe oscillations and the pressure oscillations in general take place at a much faster rate compared to the oscillation frequency. This factor could be attributed to the low mass/unit volume of the fluid, i.e. air. It can be logically expected that if the density of the fluid is more, then the damping effect of the inertia will be much more predominant and hence there would be lesser frequencies of vibration of the fluid pressure.

Secondly, the sensitivity of the system to the frequency of pipe oscillation could also be notice in the shift of frequency with maximum presence. In the frequency 4Hz case, the most dominant frequency is about 75.25. As we consider higher values of frequencies of oscillation, there is a distinct left shift of the most dominant frequency.

Thirdly, a closer look at the values of the most dominant frequencies and also the other frequencies with sharper peaks reveal that they are always some harmonics of the natural frequencies of the pipe (namely, 8.74 Hz for the first mode, 23.95 Hz for the second mode and 46.54 Hz for the third mode). Also, with increase in oscillation frequency, the value of the most dominant frequency settles around 61 Hz which is a harmonic of the first mode of natural frequency of vibration of the pipe. This is perhaps because of the reason that the pressure oscillations are "on their own" at low frequencies, but at high frequencies of oscillations, they cannot adjust to the very quick changes in the configuration of the flow domain and hence settle for some values which is maintainable at high frequencies of oscillations and thereby would be

dictated by the properties of the pipe itself. All of the above reflect a very strong coupling of the structural behaviour of the system with fluid dynamics of the flow.

One very interesting damping effect of vibration was noted at Amp4. When the frequency was increased, there was indeed a gradual left-shift in the peak frequency of pressure oscillations but the damping effect of vibration was so dominant that there was barely and fluctuation noted at low frequencies. The author concludes that this is a system dependent phenomenon and needs to be investigated with various other setups.

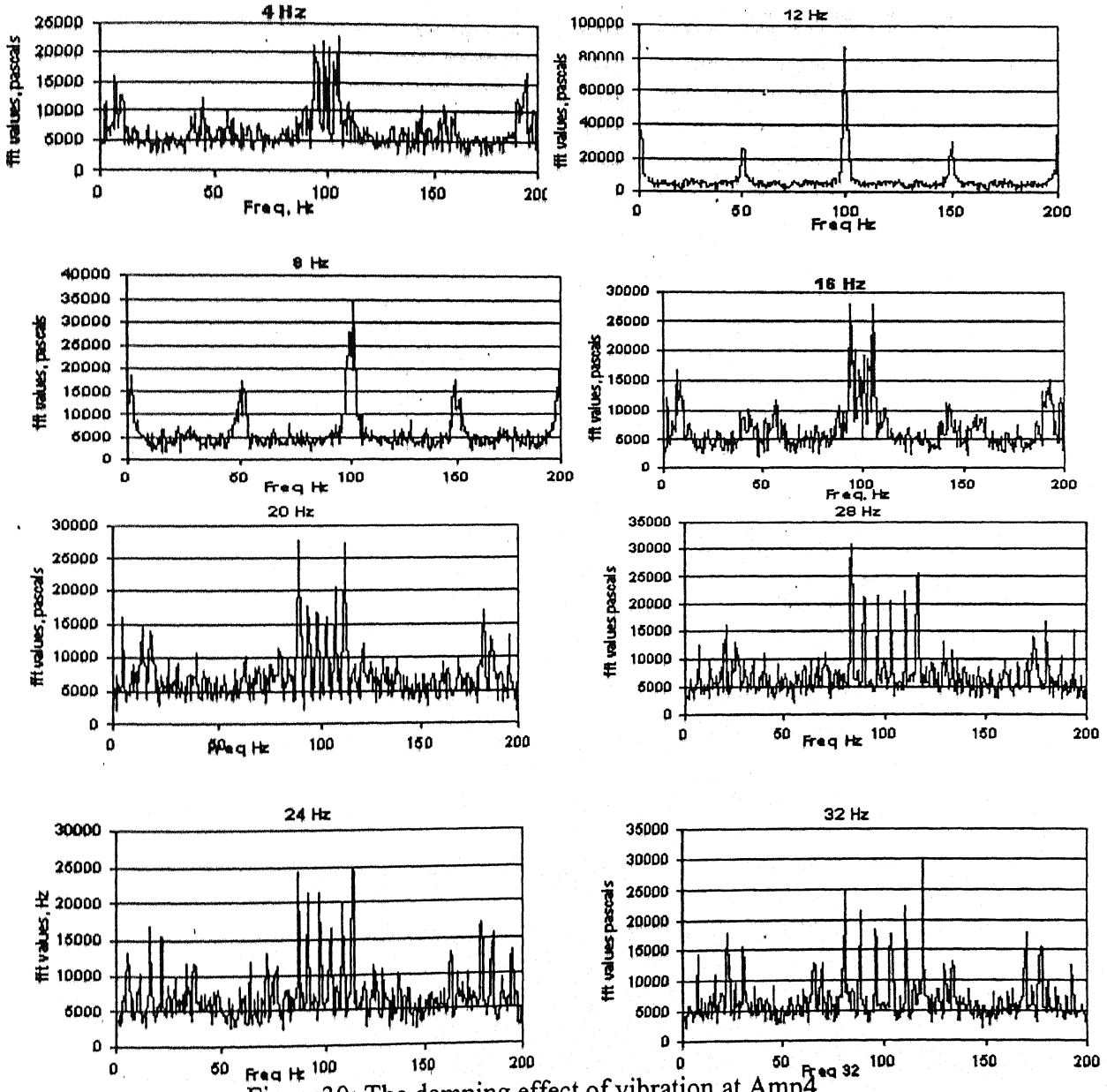

Figure30: The damping effect of vibration at Amp4

Now let us consider the other effects that the change in frequency of oscillations is having on the flow behaviour. The most important thing that is noticeable is that there is a steady drop in the mean values of pressure from the zero readings (i.e. no oscillations case). Now, since more often than not the occurrence of minimum pressure takes place at port 3, we consider the behaviour of the mean pressure there at each amplitude concerned through all the frequencies. The figures below show the same.

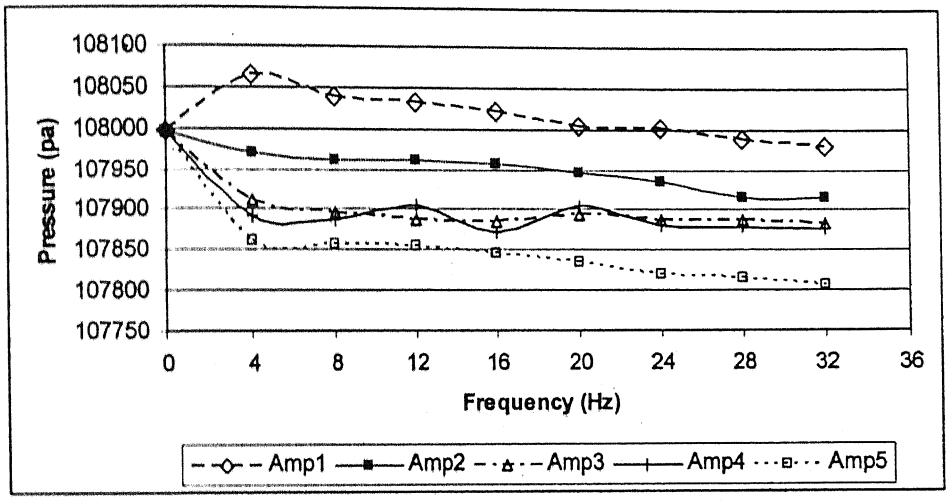

Figure31: Variation of mean pressure with frequency at various amplitudes

As can be seen from the figure above, the following two trends are there:

There can be observed a clear drop in the mean values of pressure as the amplitude of oscillation goes up. Even though these plots are for only port 3 where minimum pressure is occurring most of the times, the above observation has been found to be true for all the other ports. This can be explained in the following way. When the oscillations are taking place at freq 4, ampl, the pressure values move much faster than the domain and the effect of amplitude i.e. movement of the domain is sensed significantly by the fluid particles. As the amplitude goes up, with frequency remaining same, fluid particles have lesser and lesser time to adjust to the changes in the position of the domain and thus they adjust by means following the natural tendency of the system, i.e. with a drop in mean pressure. Now, as we mention here,

that the natural tendency of the system is to produce a drop in mean values of pressure, it seems quite logical to conclude that because, the changes in pressure in the system is basically the result of interplay of inertia (or momentum transfer), compressibility and turbulence (which always has a dissipative effect on the system). Now, normally, the inertia (or momentum transfer in the axial direction) reacts much faster to any changes in system dynamics and therefore the evacuating effect it has on the system is always more predominant than any other effect and that would obviously result in a fall of pressure in the fluid medium involved.

Now, as we can see, the fall in pressure becomes less and less precipitous with increase in frequency as the amplitude is increased. This could be explained again in the light of the statements made in the above paragraph that with increase in amplitude, the evacuating effect of the inertia is so prominent that the progressive decrease in available time with increasing frequency is having lesser and lesser effect on the fluid particles. The significance of the evacuating effect of the axial momentum transfer is also evident from the fact that as amplitude is increased, the average value of the pressure also goes down. For the prominence of this evacuating effect, we can surmise that for fluids with higher densities (i.e. water), this fall in the mean pressure values would be more prominent. And that could lead to some problems along the lines laid out in the next paragraph. This effect will be talked about again in a later paragraph.

Even though the behaviour and variations in the mean values of pressure at various ports are important, so are the nature and distribution of the drops that are taking place as well as the total fluctuations that are taking place, because they effect the flow rate directly. Fuel pumps for the modern commercial and military jet engines

are required to operate over a wide range of flow conditions, from the minimum fuel at idle descending, to the maximum fuel flow at take-off for commercial and at full after burner for military aircraft. Engine and pump drive speeds are variable over the full fuel flow range according to the mission cycles. The ratio of maximum to minimum fuel flow is referred to as "turn down" ratio. Turn down ratio of 50 plus to 1 are typical for most modern commercial jet engines and 100 to 1 are typical for most afterburner or gas generator pumps. Operating a centrifugal pump at one or two percent of its rated flow can cause excessive heating of the fuel, especially when high pressures must be generated at the rated flow. Furthermore, fast climb to high altitude makes more challenges to the pump designers because fuel temperature in tank relatively remains same during fast climbing but tank pressure drops significantly equivalent to the ambient pressure. At take-off, fuel pressure is one atmospheric pressure which is far above Vapor Pressure of fuel in most cases, but during climbing tank pressure reduces to ambient pressure at climbing altitude, which controls the maximum altitude limit unless fuel temperature and type are changed or pressurize the fuel tank. For safe flight, fuel tank pressure should be higher than vapor pressure of fuel at given temperature. The jet engine fuel has many types of dissolved gases and as the pressure reduces, the gases come out of the fuel creating two-phase flow conditions at the pump inlet. However, the aircraft has to operate at various altitudes and speeds. This will lead to different tank pressures resulting in different V/L (vapor to liquid volumetric flow ratio) at the pump inlet. However, when fuel pressure becomes close to vapor pressure, the liquid fuel becomes vaporizing to two-phase flow and fuel pump stops pumping unless specially designed to cope with this problem. Also there will be blockages in the liquid fuel passage as well. Therefore, the discharge volume of the pipeline will be severely affected. This variation in the

discharge volume will add to the variation in the flow that will be already taking place (it will be shown later) because of the vibration of the pipe. Now, this flow variation will be affected by the amount of total fluctuation (not just drop from the mean value of the no-oscillation case) that will be there in the flow. All these may ultimately severely affect the discharge volume and finally flow cut-off to the engine may take place.

Now, when we consider the nature of variation of the maximum pressure drop from zero value at any particular frequency with amplitude, as given in the figure below, we notice that the drop percentage varies almost sinusoidally, reflecting in the pattern the effect of the motion of the flow domain although nothing can be concluded from the phase differences in the curves shown.

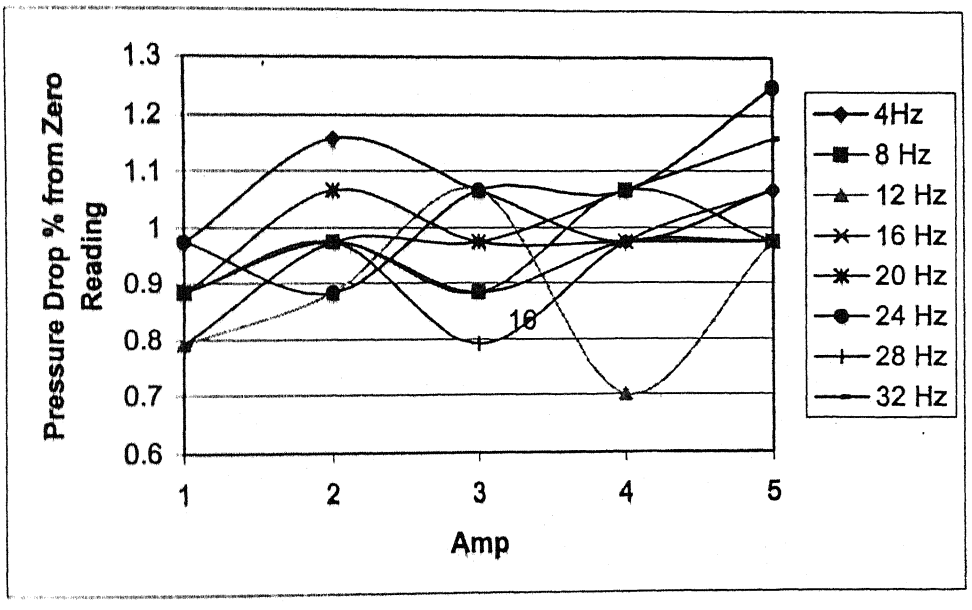

Figure32: % Variation of pressure drop with amplitude from Zero reading pressures

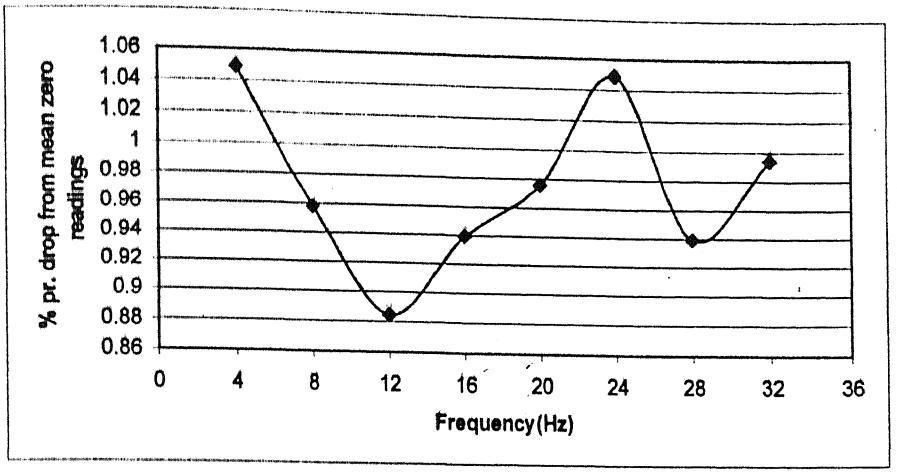

Figure33: Variation of mean pressure drop(%) with frequency

In the two figures above, the maximum drop percentage can be seen to be occurring at a frequency of 24 Hz which might be corresponding to the second bending mode of natural frequency of the pipe in oscillation.

Now, to the above curves in perspective, we also notice that as indicated in the above figure, the general trend is that there is more and more drop as amplitude of oscillation increases even though the increase is not monotonous possibly because the damping effect of the vibration becomes more prominent at various stages compared to the evacuating effect of momentum transfer.

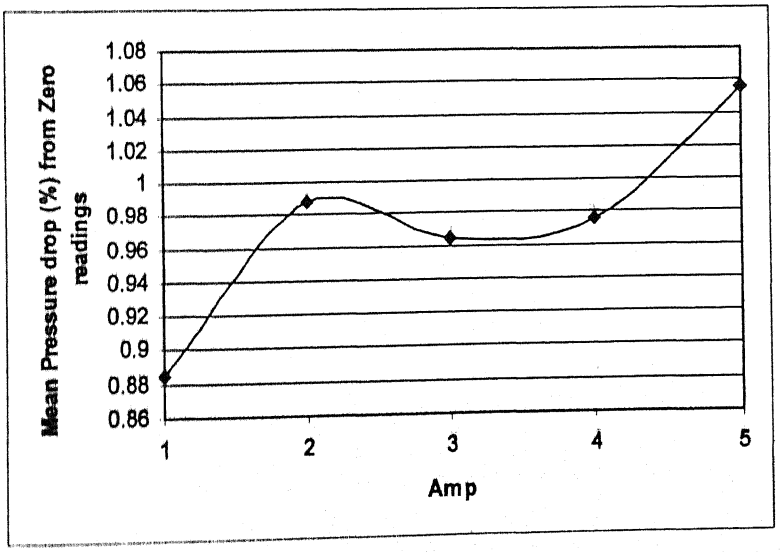

Figure34: Variation of pressure drop (%) with amplitude

So, in general it can be concluded that the maximum pressure drop effect is coming in the case of frequency 24 Hz at Amp5. One can safely expect that with fluids of higher viscosity/density, like water or kerosene, the percentage drops taking place would be more because the normally dominant evacuating effect of the momentum transport in the axial direction of the pipe would be more pronounced. That will have strong bearing in flow in cases such as in small aircraft fuel supply lines in which the fuel has a lot of dissolved substances which will come out under such drops and give the flow through the duct a pronounced two phase nature. To keep in perspective how much the pressure drops taking place, we calculate the length of piping needed for a typical fuel supply line supplying fuel to a small aircraft. Assuming a supply rate of 60 grams/minute, duct inlet diameter of 10mm, fuel density of 9 gm/cc and kinematic viscosity of 1.E-5 m^2/s, the Reynolds number is about 141 and thus at this Reynolds number to achieve a pressure drop of 1kpa, one would need, from the formula $\Delta p = \left(\frac{64}{\mathrm{Re}}\right)\left(\frac{L}{D}\right)\left(\frac{v^2}{2g}\right)$, where symbols have their usual meanings, L=2174202.13 m !! So, that much of pressure drop is very significant in case of laminar flow situations like in fuel supply lines.

Now, studies have found that there is strong interaction between total pressure fluctuations and the incoming fluid flow rate. The vibration sets in fluctuations in pressure across the fluid medium, which in turn causes fluid velocity values to fluctuate and that in effect cases the incoming fluid flow rate to fluctuate. And that is a very dangerous thing as fluctuations of even very small magnitude and frequency in the incoming flow may set up pressure fluctuations of frequencies order of magnitude higher in comparison. So, we plot the total pressure variation (maximum pressure to

minimum pressure range) as a percentage of no-oscillation values at port 6 as that is where we expect maximum variations to take place because of being farthest from the clamping spot on the pipe.

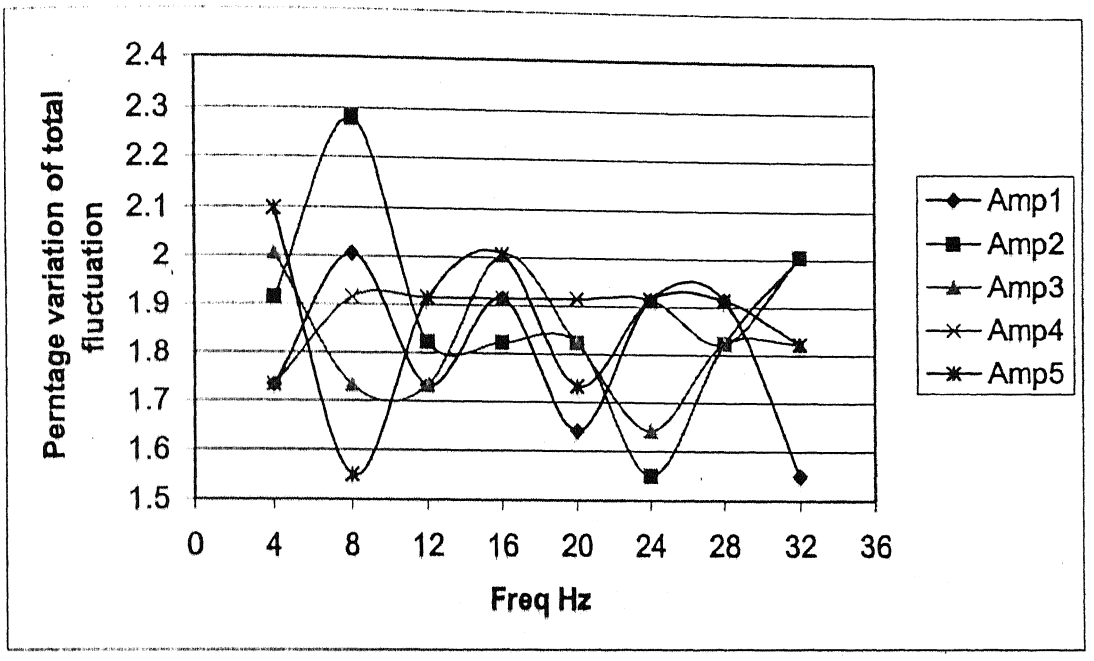

Figure 35: % Variation (w.r.t. no oscillation values) of pressure total-fluctuation with amplitude

As can be seen in the above plots the pressure total-fluctuation (max-min at any given arrangement) does not vary much with frequency at a given amplitude, whereas, we have seen that drops vary sinusoidally, which would mean that the pressure peaks take place somewhat out of phase with the drops.

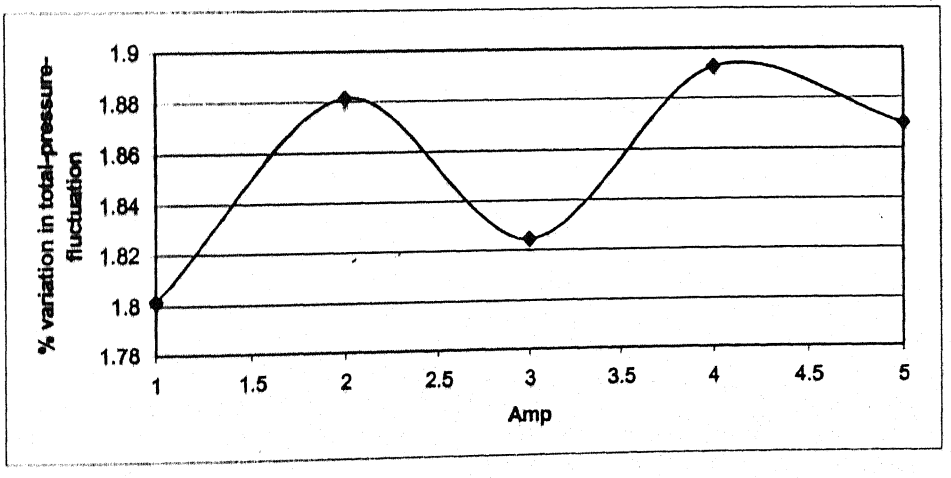

Figure 36: % Variation (w.r.t. no oscillation values) of pressure mean total-fluctuation with amplitude

As is seen with the drops, the total fluctuation also increases with increase in amplitude of oscillation and here also a minima is observed at Amp3. Possibly this amplitude has some damping effect on the pressure fluctuations which must be dependent on the flow geometry and inflow-outflow conditions.

Again, to put the significance of the pressure fluctuations in perspective, a pressure fluctuation of the order of 2 kPa would cause a local velocity fluctuation of more than 12 m/s in a fluid with physical properties like water, which will significantly affect the incoming flow as well as the discharge from the duct.

The pressure fluctuations, however, were seen to have almost zero correlation with displacement fluctuations in all cases. The following is an illustration for that.

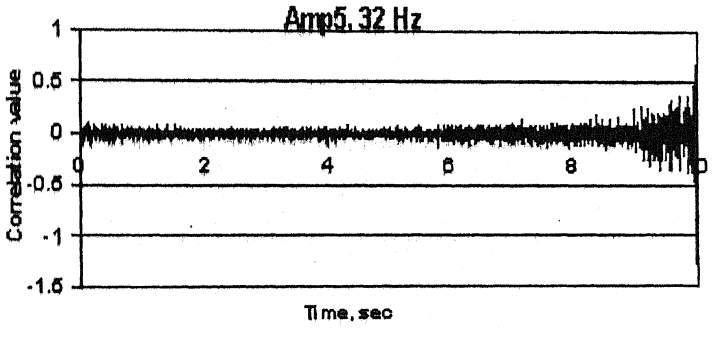

Figure37: Pressure fluctuations-displacement fluctuations correlation

The oscillations of the pipe causes changes in the pressure field inside the pipe which affects the velocity field throughout the system and therefore affects the incoming flow to oscillate as well. However, the incoming flow oscillation should

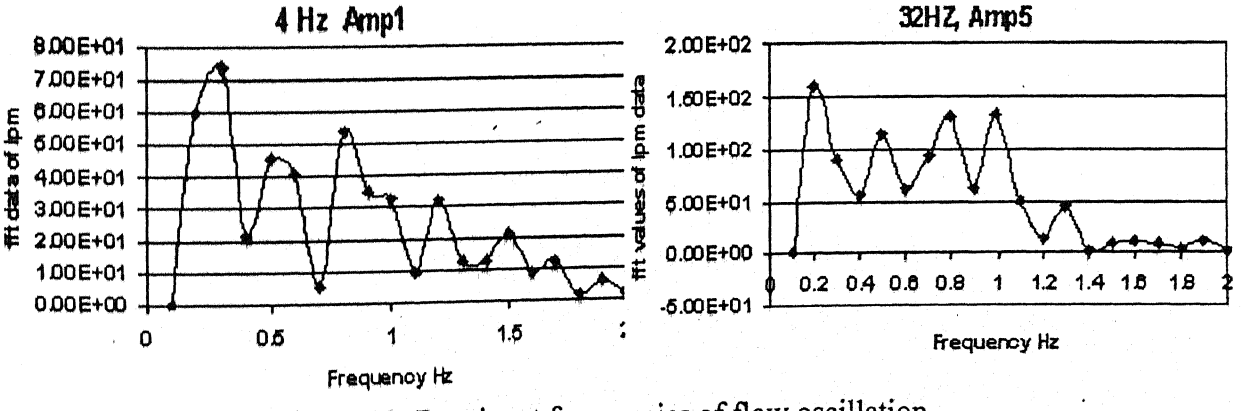

Figure 38: Dominant frequencies of flow oscillation

have oscillation frequencies much less than the pipe displacement frequencies because the incoming flow is energy assisted at a location not far away from the inlet to the pipe and therefore the incoming flow can damp out the on its own the velocity fluctuations that are transmitted to the inlet regions. The simple computational results also indicate the same in some way as there is a strict inflow boundary condition imposed at the inlet, the velocity oscillation there is much less compared to the outlet region where the flow is discharging without any adverse pressure gradient working against it.

As can be seen from above, there is not much of a variation in the frequencies of oscillation in the incoming flow with either frequency or amplitude. Frequency of oscillation in the incoming flow in general clusters in the ranges of 0.3 Hz to 0.8 Hz covering all the cases.

Now, considering the case where maximum amount of amplitude as well as maximum frequency of vibration is used, i.e. 32 Hz, Amp5 case.

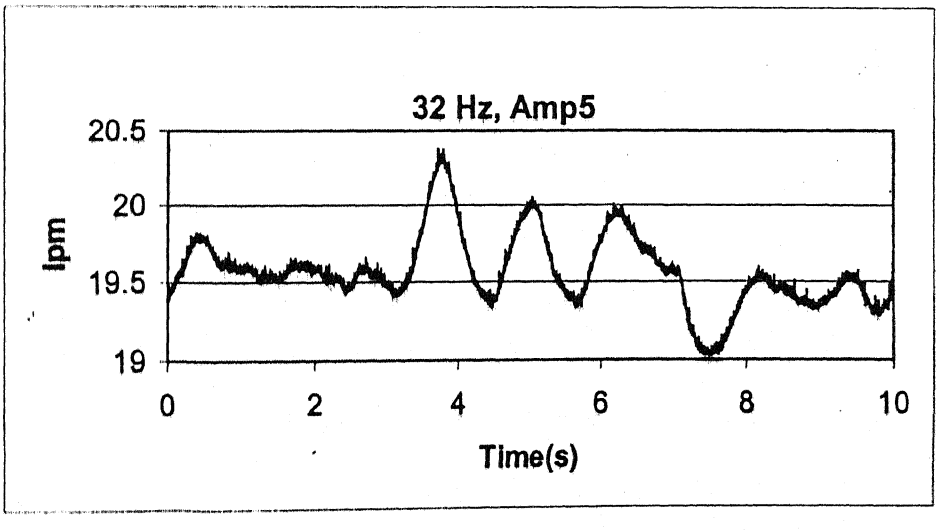

Figure 39: Flow oscillation time series plot

It can be seen that there is a maximum-minimum variation of more than 5% in the volume flow rate. In real situations with denser and more viscous fluids like

aviation fuel, more fluctuations can be affected and that would be very significant, as combustion instabilities are seen to occur at fuel volumetric flow oscillations of less than 4%. Considerations should be given to minimize the volume flow fluctuations.

Conclusions

- The pressure variation inside the pipe has a very strong relationship with the amplitude of oscillation.
- The pressure values keep on reducing as the amplitude is increased.
- The temporal variation of pressure values at any location is also effected by the amplitude and frequency of oscillation.
- There is a Left shift of frequency of pressure fluctuation with frequency of oscillation.
- High frequency pressure fluctuations set up very low frequency oscillation in the volume flow rate through the pipe.
- Flow oscillations frequencies are independent of frequency and amplitude of oscillation.
- Pressure drop pattern is affected by all of amplitude, frequency and structural effects.
- The axial velocity component is strongly affected by the oscillation and sometime flow reversals were seen to be taking place at pockets of flow at the exit.

Recommendations for Future Work:

- The pressure variations along the axial length can be captured with more resolution with greater number of sensors to have more complete ideas about axial variations along the length of the pipe.
- The pipe length should be varied to observe the structural effects it brings in and therefore helping to characterize the problem in greater details.
- The experiment needs to be carried out with more fluids, namely water etc.
- The effect of turbulence should be looked into more details.
- The study should be carried out in a two phase fluid system to see the effects on it which will have more immediate practical application.
- There is significant room for the improvement of the computer code, in terms of improvement of boundary conditions, adaptive meshing (to capture effectively flow reversals taking place inside). Various types of coordinate transformations and similar sophisticated formulations should be applied to capture the real flow physics in a moving domain problem.

REFERENCES:

[1] J.C. Misra, B. Pal, A. Pal, A.S. Gupta," Oscillatory entry flow in a plane channel with pulsating walls", International Journal of Non-Linear Mechanics 36 (2001) 731-741

[2] Kerh, Tienfuan, Lee, J., J., Wellford,L. , C. ," Finite element analysis of fluid motion with an oscillating structural system"

[3] Mateescu, D., Venditti, D.A., "Unsteady confined viscous flows with oscillating walls ans multiple separation regions over a downstream facing step", Journal of Fluids and Structures (2001) 15, 1187-1205

[4] Mateescu, D., Mekanik A., Paidoussis, P.," Analysis of unsteady annular flows with oscillating boundaries, based on a time dependent coordinate transformation", *Journal of Fluids and Structures* (1996) **10** , 57 – 77

[6] Benhamou, B., Laneville, A., Galanis, N.," Transition to turbulence: the case of a pipe in radial oscillation", International Journal of Thermal Sciences 43 (2004) 1141–1151

[7] Ozdinc, M. , Arpinlioglu, C., Yas, M., Gu¨ndog˘du, A.," A critical review on pulsatile pipe flow studies directing towards future research topics", Flow Measurement and Instrumentation 12 (2001) 163–174

[8] Tjjiseling, T., " Fluid structure interaction in liquid filled pipe systems: a review", *Journal of Fluids and Structures* (1996) **10** , 109 – 146

[9] Ghia, U., Ghia, N. k., Shin, C.T., "High-Re solutions for incompressible flow using the Navier-Stokes equations and a multigrid method", Journal of Computational Physics,48, 387-411.

[10] White, F., M., "Viscous Fluid Flow", second Edition, McGraw-Hill Inc.